JEM Journal of Experimental Medicine

ARTICLE

AIM2 regulates anti-tumor immunity and is a viable therapeutic target for melanoma

Keitaro Fukuda[1,4], Ken Okamura[1], Rebecca L. Riding[1], Xueli Fan[1], Khashayar Afshari[1], Nazgol-Sadat Haddadi[1], Sean M. McCauley[2], Mehmet H. Guney[2], Jeremy Luban[2,3], Takeru Funakoshi[4], Tomonori Yaguchi[5], Yutaka Kawakami[5], Anastasia Khvorova[6,7], Katherine A. Fitzgerald[8], and John E. Harris[1]

The STING and absent in melanoma 2 (AIM2) pathways are activated by the presence of cytosolic DNA, and STING agonists enhance immunotherapeutic responses. Here, we show that dendritic cell (DC) expression of AIM2 within human melanoma correlates with poor prognosis and, in contrast to STING, AIM2 exerts an immunosuppressive effect within the melanoma microenvironment. Vaccination with AIM2-deficient DCs improves the efficacy of both adoptive T cell therapy and anti–PD-1 immunotherapy for "cold tumors," which exhibit poor therapeutic responses. This effect did not depend on prolonged survival of vaccinated DCs, but on tumor-derived DNA that activates STING-dependent type I IFN secretion and subsequent production of CXCL10 to recruit CD8⁺ T cells. Additionally, loss of AIM2-dependent IL-1β and IL-18 processing enhanced the treatment response further by limiting the recruitment of regulatory T cells. Finally, AIM2 siRNA-treated mouse DCs in vivo and human DCs in vitro enhanced similar anti-tumor immune responses. Thus, targeting AIM2 in tumor-infiltrating DCs is a promising new treatment strategy for melanoma.

Introduction

Melanoma is an aggressive skin cancer with high mortality in those with advanced disease. However, melanoma is particularly immunogenic, increasing its susceptibility to immunotherapy. The advent of adoptive T cell therapy (ACT) and anti–PD-1 antibody (Ab) therapy has improved the prognosis of patients with stage IV melanoma. However, durable responses to these therapies are limited to 35–45% of patients (Goff et al., 2016; Robert et al., 2019), representing a significant unmet need for those not responding to current immunotherapies.

The success of immunotherapy strongly correlates with the number of tumor-infiltrating CD8⁺ T cells before therapy (Tumeh et al., 2014). A melanoma infiltrated by a large number of CD8⁺ T cells, referred to as a "hot tumor" due to the amount of inflammation present, responds well to immunotherapies, while a tumor infiltrated by few CD8⁺ T cells, referred to as a "cold tumor," typically shows a poor response (Spranger et al., 2017). The infiltration of CD8⁺ T cells into tumors is facilitated by the recognition of tumor-derived DNA by the cytosolic cGAS–STING (cyclic guanosine monophosphate-adenosine monophosphate synthase–stimulator of IFN genes) signaling pathway in tumor-infiltrating dendritic cells (TIDCs; Deng et al., 2014; Woo et al., 2014). This leads to type I IFN production by TIDCs and promotes their migration to the tumor-draining LN (TdLN). There, they prime tumor antigen-specific T cells and promote their migration to the tumor (Corrales et al., 2017). In this setting, STING agonists are being tested in clinical trials as an adjuvant immunotherapy for advanced melanoma (Li et al., 2017).

While the importance of the cGAS–STING signaling pathway in TIDCs is well established, tumor-derived cytosolic DNA can also be recognized by absent in melanoma 2 (AIM2). AIM2 was initially identified as a gene whose expression was lost in melanoma cells (DeYoung et al., 1997). Despite its name, the function of AIM2 in the melanoma microenvironment is unknown. AIM2 is a cytosolic double-stranded DNA-binding protein that forms a caspase-1–activating inflammasome complex, resulting in proteolytic processing of the inflammatory cytokines IL-1β and IL-18 and the pore-forming protein gasdermin D, which elicits a lytic form of cell death called pyroptosis (Man et al., 2016). IL-1β expression positively correlates with melanoma thickness (Qin et al., 2011), suggesting that the cytokine promotes tumor

[1]Department of Dermatology, University of Massachusetts Medical School, Worcester, MA; [2]Program in Molecular Medicine, University of Massachusetts Medical School, Worcester, MA; [3]Department of Biochemistry and Molecular Pharmacology, University of Massachusetts Medical School, Worcester, MA; [4]Department of Dermatology, Keio University School of Medicine, Tokyo, Japan; [5]Division of Cellular Signaling, Institute for Advanced Medical Research, Keio University School of Medicine, Tokyo, Japan; [6]RNA Therapeutics Institute, University of Massachusetts Medical School, Worcester, MA; [7]Department of Molecular Medicine, University of Massachusetts Medical School, Worcester, MA; [8]Department of Infectious Diseases and Immunology, University of Massachusetts Medical School, Worcester, MA.

Correspondence to John E. Harris: John.Harris@umassmed.edu; Keitaro Fukuda: kei_fu@keio.jp.

growth. Notably, most melanoma cells silence expression of one or more inflammasome components and do not produce IL-1β by themselves but instead induce IL-1β production from tumor-associated macrophages (MACs) by releasing endogenous danger signals (Gehrke et al., 2014). IL-18 also belongs to the IL-1 family of cytokines and activates the MyD88–NF-κB signaling pathway (Kaplanski, 2018); however, its effect on melanoma growth is nuanced. Treatment with IL-18 has been reported to suppress melanoma growth and metastasis (Fabbi et al., 2015; Ma et al., 2016) but also accelerate melanoma growth by accumulating monocytic myeloid-derived suppressor cells in the melanoma microenvironment (Lim et al., 2014). In addition, AIM2 has also been reported to suppress the STING signaling axis in murine bone marrow–derived dendritic cells (BMDCs) and bone marrow–derived MACs in response to tumor-derived cytosolic DNA in vitro (Banerjee et al., 2018; Corrales et al., 2016). Considering the nuanced effects of cytoplasmic nucleic acid sensing within the tumor microenvironment, we sought to determine what role, if any, AIM2 plays during the tumor immune response.

Here, we report that AIM2 expression correlates with tumor progression in human melanoma patients and functions as a negative regulator of the STING pathway within TIDCs. Eliminating AIM2 signaling during dendritic cell (DC) vaccination by using either AIM2-deficient (*Aim2*$^{-/-}$) BMDCs or siRNA-mediated knockdown of AIM2 before treatment improved the efficacy of both ACT and anti–PD-1 immunotherapy. Antigen-loaded, *Aim2*$^{-/-}$ BMDCs migrated to the tumor and promoted CD8$^+$ T cell infiltration through the production of CXCL10 while limiting the accumulation of regulatory T cells (T reg cells), thus making cold tumors hot. This effect required STING–type I IFN signaling and was only partially recapitulated using *Il1β*$^{-/-}$ or *Il18*$^{-/-}$ DC vaccines. Furthermore, AIM2 siRNA-transfected human monocyte-derived DCs (MoDCs) stimulated with tumor-derived DNA demonstrated an increased inflammatory response, similar to mouse *Aim2*$^{-/-}$ BMDCs. Collectively, our data indicate that an AIM2 siRNA-transfected DC vaccine could be an effective strategy to improve the efficacy of melanoma immunotherapy by promoting STING-induced type I IFN secretion, as well as limiting IL-1β and IL-18 production.

Results

AIM2 restricts anti-melanoma immunity within the melanoma microenvironment

To determine whether AIM2 in the melanoma microenvironment regulates melanoma progression, we s.c. challenged WT and *Aim2*$^{-/-}$ mice with B16F10, a poorly immunogenic melanoma cell line that does not express Aim2 mRNA (Znidar et al., 2016) and that is resistant to anti–PD-1 Ab therapy (Homet Moreno et al., 2016). We found that *Aim2*$^{-/-}$ mice exhibited slower tumor growth than WT mice (Fig. 1 A). Within the tumor, numbers of CD8$^+$ or CD4$^+$ T cells, MACs, total DCs, CD103$^+$ DCs, or CD11b$^+$ DCs did not differ between WT and *Aim2*$^{-/-}$ mice, whereas *Aim2*$^{-/-}$ mice had a smaller proportion of T reg cells, a larger proportion of CD4$^+$ effector T cells (CD4$^+$ Teffs), and higher CD8/T reg cell ratio compared with WT mice (Fig. 1, B and C; and Fig. S1 B). Numbers of CD8$^+$ or CD4$^+$ T cells and proportions of T reg cells in the TdLN or spleen did not differ between WT and *Aim2*$^{-/-}$ mice (Fig. S1 C). To test whether cytokines known to support anti-tumor immunity are induced in *Aim2*$^{-/-}$ mice, we measured the percentage of IFN-γ– or TNF-α–producing CD8$^+$ T cells and concentration of IFN-β, IL-1β, and IL-18 in the tumor. There was no difference in the percentage of IFN-γ– or TNF-α–producing CD8$^+$ T cells within the tumor (Fig. 1 D), whereas the B16F10 tumor in *Aim2*$^{-/-}$ mice had a higher amount of IFN-β and a lower amount of IL-1β and IL-18 compared with those of WT mice (Fig. 1, E and F). These results indicate that AIM2 plays an immunosuppressive role within the melanoma microenvironment.

Similarly, another poorly immunogenic melanoma cell line, YUMM1.7 (Homet Moreno et al., 2016), grew more slowly in *Aim2*$^{-/-}$ mice than in WT mice (Fig. 1 G). *Aim2*$^{-/-}$ mice had a higher number of CD8$^+$ T cells, a smaller proportion of T reg cells, a larger proportion of CD4$^+$ Teffs, and a higher CD8/T reg cell ratio in the tumor than WT mice, whereas there was no difference in the numbers of CD4$^+$ T cells, MACs, total DCs, CD103$^+$DCs, or CD11b$^+$DCs (Fig. 1, H and I; and Fig. S1 D). Numbers of CD8$^+$ or CD4$^+$ T cells or proportion of T reg cells in the TdLN or spleen also did not differ between WT and *Aim2*$^{-/-}$ mice (Fig. S1 E). Furthermore, there was no difference in the percentage of IFN-γ– or TNF-α–producing CD8$^+$ tumor-infiltrating lymphocytes (TILs) between WT and *Aim2*$^{-/-}$ mice (Fig. 1 J), whereas the YUMM1.7 tumor in *Aim2*$^{-/-}$ mice had a higher amount of IFN-β and a lower amount of IL-1β and IL-18 than those of WT mice (Fig. 1, K and L), similar to B16F10 melanomas reported above. These results demonstrate that the immunosuppressive effect of AIM2 in the melanoma microenvironment is not limited to the B16F10 model.

AIM2 expression in human melanoma–infiltrating DCs correlates with tumor progression

In melanoma, TIDCs are the major producers of IFN-β (Deng et al., 2014), and we found that *Aim2*$^{-/-}$ mice had greater amounts of IFN-β in implanted melanomas compared with those of WT mice. Therefore, we next addressed whether AIM2 is expressed in DCs infiltrating human melanoma tissue and whether AIM2 expression correlates with tumor progression. To test this, we quantified the expression of AIM2 and CD11c on histological sections of primary lesions of 31 melanoma patients (Table 1). Although the density of CD11c$^+$ cells were similar between thin (≤2.00 mm, T1 and T2) and thick (>2.00 mm, T3 and T4) cutaneous melanomas, thick melanomas had a higher density and proportion of AIM2-expressing CD11c$^+$ cells compared with thin melanomas (Fig. 1, M and N). Similarly, the densities of CD141$^+$ and CD1c$^+$ cells were similar between thin and thick cutaneous melanomas, whereas thick melanomas had a higher density of AIM2-expressing CD141$^+$ and CD1c$^+$ cells compared with thin melanomas (Fig. S1, F and G). These findings indicate that AIM2-expressing TIDCs are increased in patients with melanoma and correlate with tumor progression.

DC vaccination is enhanced by AIM2-deficient DCs and is mediated by STING–type I IFN signaling

Since tumor-derived cytosolic DNA is known to activate the cGAS–STING pathway to produce type I IFN in TIDCs, we examined

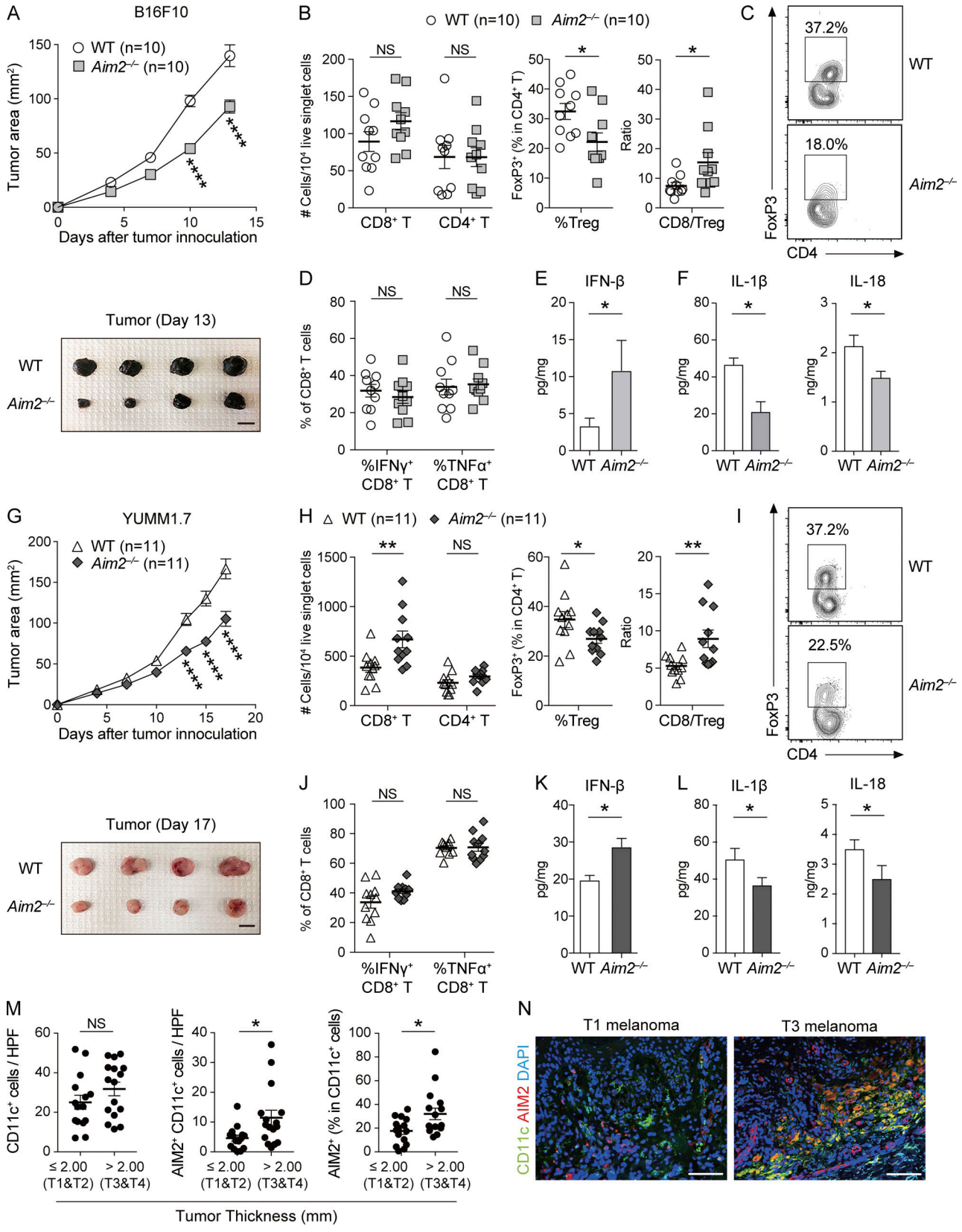

Figure 1. **AIM2 exerts an immunosuppressive effect in the melanoma microenvironment. (A–F)** WT and *Aim2*$^{-/-}$ mice were inoculated s.c. with 1.0 × 10^6 B16F10 cells on day 0. On day 13, tissues were harvested. **(A)** Tumor growth over time (top; *n* = 10). Sample photo of B16F10 tumor on day 13 (bottom). Scale bar, 10 mm. **(B–D)** Flow cytometry analysis of TILs (*n* = 10). **(B)** The numbers of CD8$^+$ and CD4$^+$ T cells among 10^4 live singlet cells. Percentage of FoxP3$^+$ cells in CD4$^+$ T cells and CD8/T reg cell ratio. **(C)** Representative contour plot for FoxP3 among CD4$^+$ T cells. **(D)** Percentages of IFN-γ$^+$ and TNF-α$^+$ in CD8$^+$ T cells.

(E and F) IFN-β (n = 7; E), IL-1β, and IL-18 (n = 6; F) protein levels within the tumor. **(G–L)** WT and *Aim2*$^{-/-}$ mice were inoculated s.c. with 1.0 × 10^6 YUMM1.7 cells on day 0. On day 17, tissues were harvested. **(G–J)** Similar analysis as in A–D was performed on YUMM1.7 tumor–bearing WT and *Aim2*$^{-/-}$ mice (n = 11). **(G)** Tumor growth over time (top; n = 11). Sample photo of YUMM1.7 tumor on day 17 (bottom). Scale bar, 10 mm. **(K and L)** IFN-β (n = 8; K), IL-β, and IL-18 (n = 7; L) protein levels within the tumor. **(M)** The numbers of CD11c$^+$ and AIM2$^+$CD11c$^+$ cells and the percentage of AIM2$^+$ cells in CD11c$^+$ cells in HPF of primary lesions of human thin (n = 15) and thick (n = 16) melanomas. **(N)** Immunofluorescence microscopy of primary lesions of human thin and thick primary melanomas, visualized for CD11c, AIM2, and DAPI. Scale bar, 100 µm. Data are shown as mean ± SEM and are pooled from four (M), three (A, B, D, G, H, and J), or two (E, F, K, and L) experiments or are representative of at least three independent experiments (C, I, and N). *, P < 0.05; **, P < 0.01; ****, P < 0.0001; two-way ANOVA with Sidak's multiple-comparisons test (A and G) or Mann–Whitney test (B, D–F, H, and J–M).

the role of AIM2 in controlling these responses in vitro by stimulating BMDCs with B16F10-derived DNA (B16F10 DNA), delivered via lipofection. The levels of mRNA for IFN-β and IFN-α as well as the IFN-regulated chemokines CXCL10 and CXCL9 were all increased in *Aim2*$^{-/-}$ BMDCs compared with those in WT BMDCs in response to B16F10 DNA. Furthermore, in agreement with previous studies (Banerjee et al., 2018; Corrales et al., 2016), WT and *Aim2*$^{-/-}$ BMDCs induced IFN-β and CXCL10 production in a dose-dependent manner, and *Aim2*$^{-/-}$ BMDCs secreted more IFN-β and CXCL10 than WT BMDCs following stimulation with B16F10 DNA. These responses were all abolished in *Aim2*$^{-/-}$*Sting*$^{-/-}$ BMDCs and *Sting*$^{-/-}$ BMDCs, indicating that AIM2 in BMDCs inhibits the production of type I IFN and IFN-stimulated gene products in response to tumor-derived DNA through STING (Fig. 2 A and Fig. S2 A), consistent with earlier observations (Banerjee et al., 2018; Rathinam et al., 2010). Indeed, following stimulation with B16F10 DNA, *Aim2*$^{-/-}$ BMDCs showed enhanced phosphorylation of TBK1 (pTBK1) and IRF3 (pIRF3), proteins downstream of STING–type I IFN signaling, compared with WT BMDCs. These responses were abolished in *Aim2*$^{-/-}$*Sting*$^{-/-}$ and *Sting*$^{-/-}$ BMDCs, suggesting that AIM2 inhibits STING–type I IFN signaling in response to tumor-derived DNA in BMDCs (Fig. 2 B).

Table 1. **Characteristics of patients analyzed in this study**

	N
Sex	
Male	11
Female	20
Age (yr)	
Mean ± SD	59.8 ± 16.3
Median (range)	64.0 (15–88)
Primary lesion	31
Tumor thickness	
<1.00 mm	10
1.00–2.00 mm	5
2.01–4.00 mm	7
>4.01 mm	9
Mean ± SD (mm)	3.04 ± 2.89
Median (range)	2.10 (0.2–10.0)
Tumor subtype	
Acral lentiginous melanoma	10 (32.3%)
Nodular melanoma	11 (35.5%)
Superficial spreading melanoma	9 (29.0%)
Lentigo maligna melanoma	1 (3.2%)
TNM stage	
Stage I	12
Stage II	9
Stage III	9
Stage IV	1

Given the enhanced activation of STING–type I IFN signaling in *Aim2*$^{-/-}$ BMDCs in response to tumor-derived DNA, we next examined the functional role of AIM2 in DCs during ACT in vivo. To evaluate whether *Aim2*$^{-/-}$ DC vaccination can be used to enhance the anti-melanoma immunity of immunotherapies, we administered hgp100 peptide-pulsed BMDCs (DC-gp100) with ACT, a combination therapy of radiation, IL-2, and adoptively transferred T cells. The T cells were transgenic for Thy1.1, as well as a TCR that recognizes gp100 (also called premelanosome protein, or PMEL), a tumor-specific antigen in B16F10 melanoma (Fig. 2 C). Using CD45.1 B6 mice as hosts, we observed that i.v. injected DCs (CD11c$^+$ MHC-II$^+$ Thy1.1$^-$CD45.2$^+$ cells) migrated into the tumor, TdLN, and spleen within 1.5 d after injection, with the highest number in the spleen, and this was unaffected by AIM2 deficiency (Fig. S2, B and C).

Consistent with previous reports (Lou et al., 2004), the combination of DC vaccination with ACT led to a more robust anti-tumor response than ACT alone. Among mice receiving ACT with DC-gp100, those receiving *Aim2*$^{-/-}$ DC-gp100 exhibited lower tumor burden than WT and *Aim2*$^{-/-}$*Sting*$^{-/-}$ DC-gp100 (Fig. 2 D). Within the tumor, hosts receiving *Aim2*$^{-/-}$ DC-gp100 had higher numbers of gp100-specifc CD8$^+$ T cells (hereinafter referred to as "PMELs"), CD8$^+$ T cells, a lower proportion of T reg cells, a higher proportion of CD4$^+$ Teffs, and higher PMELs-to-T reg cell ratio (hereinafter referred to as "PMEL/T reg cell ratio") than those receiving WT and *Aim2*$^{-/-}$*Sting*$^{-/-}$ DC-gp100, whereas there was no difference in the numbers of CD4$^+$ T cells, MACs, total DCs, CD103$^+$DCs, CD11b$^+$DCs, or percentage of IFN-γ– or TNF-α–producing PMELs among the groups (Fig. 2, E and F; and Fig. S2 D). Furthermore, there were more PMELs in the spleen in hosts receiving *Aim2*$^{-/-}$ DC-gp100, whereas the number of PMELs in the TdLN, numbers of CD8$^+$ or CD4$^+$ T cells, or proportion of T reg cells in the TdLN and spleen did not differ among the three groups (Fig. S2 E). Together, these results indicate that *Aim2*$^{-/-}$ DC vaccination improves the efficacy of ACT, and the enhanced anti-melanoma immunity of *Aim2*$^{-/-}$ DC vaccine is dependent on STING signaling.

To examine in which tissue ACT with *Aim2*$^{-/-}$ DC-gp100 induced type I IFN production, we examined the amount of IFN-β

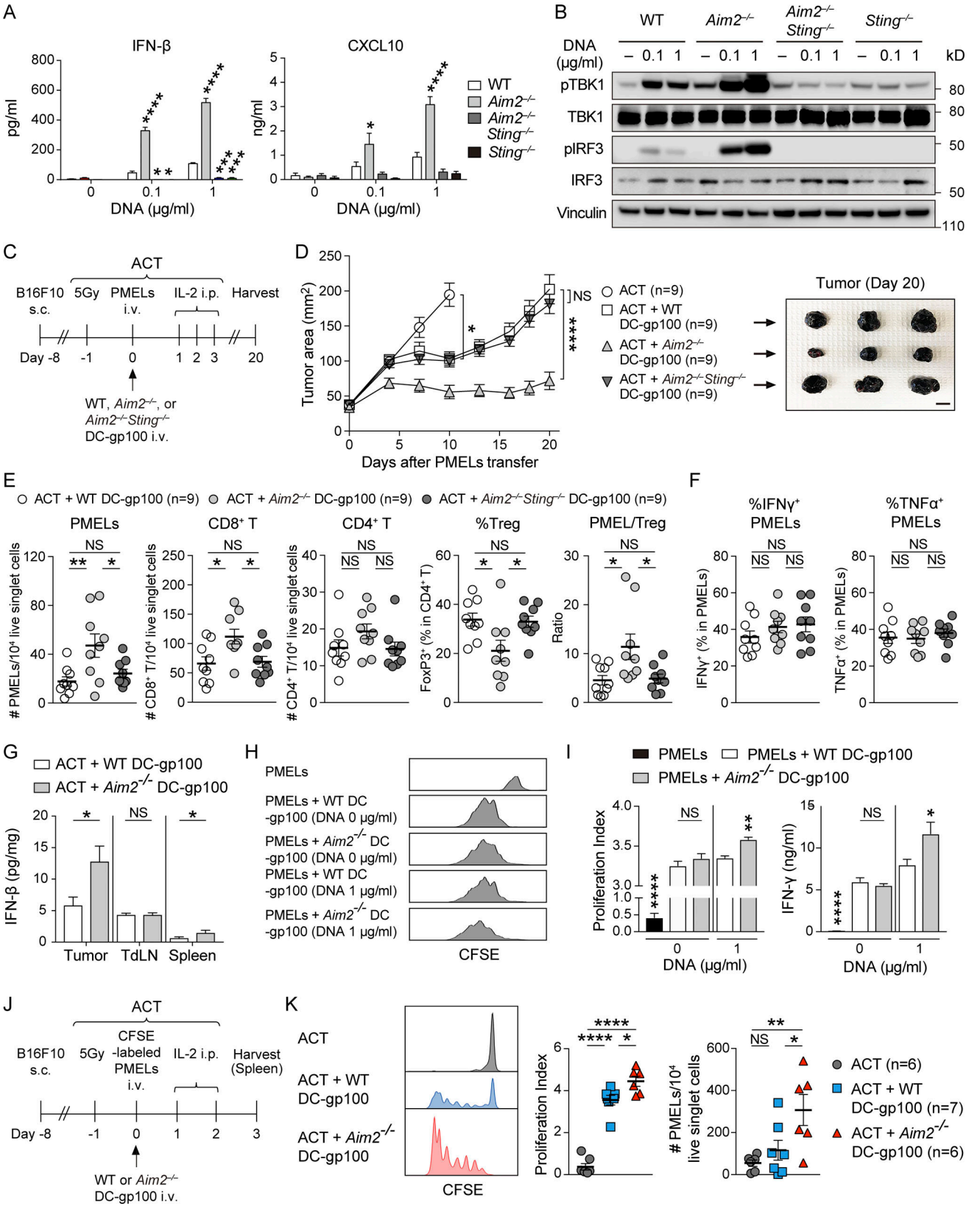

Figure 2. **Vaccination with AIM2-deficient DC improves the efficacy of ACT through activation of STING–type I IFN signaling. (A)** IFN-β or CXCL10 in the supernatants of indicated BMDCs stimulated with 0, 0.1, or 1 μg/ml B16F10 DNA for 4 h (IFN-β) or 10 h (CXCL10; *n* = 3). **(B)** Immunoblotting for pTBK1, TBK1, pIRF3, IRF3, and vinculin in the lysates of indicated BMDCs stimulated with 0, 0.1, or 1 μg/ml B16F10 DNA for 4 h. **(C–G)** B16F10-bearing WT mice (B16F10 mice) were treated with ACT alone or ACT + 1.0 × 10^6 WT, *Aim2*$^{-/-}$, or *Aim2*$^{-/-}$*Sting*$^{-/-}$ DC-gp100. On day 20 after PMELs (1.0 × 10^6 cells) transfer, tissues were harvested. **(C)** The therapy regimen scheme. **(D)** Tumor growth over time (left; *n* = 9). Sample photo of B16F10 tumor on day 20 after PMELs

transfer (right). Scale bar, 10 mm. **(E and F)** Flow cytometry analysis of TILs (n = 9). **(E)** The numbers of PMELs, $CD8^+$ T cells, and $CD4^+$ T cells among 10^4 live singlet cells, percentage of $FoxP3^+$ cells in $CD4^+$ T cells, and PMEL/T reg cell ratio. **(F)** Percentages of IFN-γ^+ and TNF-α^+ cells in PMELs. **(G)** IFN-β protein levels within the tumor, TdLN, and spleen (n = 7). **(H and I)** B16F10 DNA–stimulated WT or *Aim2*$^{-/-}$ DC-gp100 was cocultured with CFSE-labeled PMELs for 72 h (n = 5). **(H)** Histograms of PMELs CFSE dilution. **(I)** Proliferation index of PMELs and amount of IFN-γ^+ in the supernatants. **(J and K)** B16F10 mice were treated with ACT using 1.0 × 10^6 CFSE-labeled PMELs + 1.0 × 10^6 WT or *Aim2*$^{-/-}$ DC-gp100. On day 3 after PMELs transfer, spleens were harvested. **(J)** The therapeutic regimen. **(K)** Histograms of PMELs CFSE dilution, proliferation index of PMELs, and numbers of PMELs among 10^4 live singlet cells in the spleen (n = 6 or 7). Data are shown as mean ± SEM and are pooled from three (A and D–G) or two (I and K) experiments or are representative of at least two independent experiments (B, H, and K). *, P < 0.05; **, P < 0.01; ***, P < 0.001; ****, P < 0.0001; two-way ANOVA with Tukey's multiple-comparisons test (D), one-way ANOVA with Dunnett's (A and I) or Tukey's (E, F, and K) multiple-comparisons test, or Mann–Whitney test (G and I).

in the tumor, TdLN, and spleen of mice treated by ACT with WT or *Aim2*$^{-/-}$ DC-gp100. Consistent with the numbers of PMELs in each tissue, the amount of IFN-β was higher in the tumor and spleen of hosts receiving *Aim2*$^{-/-}$ DC-gp100 than in hosts receiving WT DC-gp100, whereas there was no difference in the TdLNs between the two groups. Notably, the amount of IFN-β was highest in the tumor, followed in order by the TdLN and spleen (Fig. 2 G).

Since type I IFN is known to promote T cell priming, we next examined the effect of *Aim2*$^{-/-}$ DC-gp100 on priming PMELs by coculturing WT or *Aim2*$^{-/-}$ DC-gp100 with PMELs. Expression of the DC markers CD11b and CD103 was similar between WT and *Aim2*$^{-/-}$ DC-gp100, whereas *Aim2*$^{-/-}$ DC-gp100 had higher expression of MHC-I and costimulatory signals CD86 and CD80 compared with WT DC-gp100 (Fig. S2, F and G). The proliferation index of PMELs and the amount of IFN-γ in the supernatant were higher in PMELs cocultured with B16F10 DNA–treated *Aim2*$^{-/-}$ DC-gp100 than in B16F10 DNA–treated WT DC-gp100, whereas there was no difference between PMELs cocultured with B16F10 DNA–nontreated WT and *Aim2*$^{-/-}$ DC-gp100 (Fig. 2, H and I). These results were further supported by an in vivo PMELs priming assay, where B16F10 mice treated with ACT with *Aim2*$^{-/-}$ DC-gp100 showed a higher number and proliferation index of PMELs in the spleen compared with B16F10 mice treated with ACT with WT DC-gp100 (Fig. 2, J and K). Collectively, these results indicate that *Aim2*$^{-/-}$ DC vaccination has a stronger impact on priming of PMELs in the spleen with regard to cell numbers and proliferation compared with WT DC vaccination.

Enhanced anti-melanoma immunity of AIM2-deficient DC vaccination depends on the recognition of tumor-derived DNA, but not on prolonged survival of introduced DCs

To determine whether enhanced anti-melanoma immunity of *Aim2*$^{-/-}$ DC vaccine depends on the recognition of tumor-derived DNA, we performed ACT with DC vaccination while injecting the tumor with DNase I (Fig. 3 A). The therapeutic effect of *Aim2*$^{-/-}$ DC-gp100 on ACT was abrogated in mice intratumorally administered DNase I (Fig. 3 B). Tumors injected with DNase I contained fewer PMELs and $CD8^+$ T cells, a higher proportion of T reg cells, and a smaller PMEL/T reg cell ratio than tumors injected with PBS (Fig. 3 C). Furthermore, intratumoral DNase I treatment decreased the numbers of PMELs in TdLN and spleen, whereas total $CD8^+$, $CD4^+$ T cells, and the proportion of T reg cells were unchanged (Fig. S3, A and B). These results demonstrate that the enhanced anti-tumor immunity of the *Aim2*$^{-/-}$ DC vaccine depends on the recognition of tumor-derived DNA.

AIM2 senses the presence of cytosolic DNA and thereby can induce pyroptosis of the cell. We sought to determine whether suppression of pyroptosis leads to prolonged survival in *Aim2*$^{-/-}$ DC-gp100, thereby increasing the number of tumor-infiltrating DC vaccines. To test this, we performed ACT with WT or *Aim2*$^{-/-}$ DC-gp100 into a CD45.1 host and quantified the vaccinated DCs infiltrating the tumor at 10 and 20 d after transfer of PMELs (Fig. 3, D–F). Similar to the tumor analyzed at 1.5 d after transfer of PMELs (Fig. S2 C), there was no difference in the number of vaccinated DCs infiltrating the tumor, TdLN, or spleen. These results indicate that enhanced anti-tumor immunity of the *Aim2*$^{-/-}$ DC vaccine does not depend on prolonged survival of the DC vaccine.

AIM2-deficient DC vaccination requires autologous type I IFN signaling and promotes tumor antigen–specific $CD8^+$ T cell infiltration into the tumor via CXCL10

As shown earlier, *Aim2*$^{-/-}$ BMDCs produce greater amounts of IFN-β and CXCL10 than WT BMDCs following in vitro stimulation with tumor DNA. This enhanced cytokine production in *Aim2*$^{-/-}$ BMDCs was dependent on type I IFN signaling, since these responses were impaired in *Aim2*$^{-/-}$*Ifnar*$^{-/-}$ BMDCs (Fig. 4 A). These results suggest that autocrine type I IFN signaling in BMDCs is required for the enhanced inflammatory function of the *Aim2*$^{-/-}$ DC vaccine.

We next sought to determine whether autologous type I IFN signaling and CXCL10 production were required for enhanced anti-tumor immunity by the *Aim2*$^{-/-}$ DC vaccine in vivo. To test this, we performed ACT with *Aim2*$^{-/-}$*Ifnar*$^{-/-}$ or *Aim2*$^{-/-}$*Cxcl10*$^{-/-}$ DC-gp100. Vaccination with *Aim2*$^{-/-}$*Ifnar*$^{-/-}$ DC eliminated the enhanced anti-tumor effect of *Aim2*$^{-/-}$ DC vaccination, such that hosts receiving *Aim2*$^{-/-}$*Ifnar*$^{-/-}$ DC-gp100 experienced similar tumor growth as those receiving WT DC-gp100. Similarly, but to a lesser extent, *Aim2*$^{-/-}$*Cxcl10*$^{-/-}$ DC-gp100 revealed a decreased anti-tumor effect (Fig. 4 B). Within the tumor, hosts receiving *Aim2*$^{-/-}$ DC-gp100 had higher numbers of PMELs and $CD8^+$ T cells than other groups, whereas there was no difference in numbers of $CD4^+$ T cells, $CD103^+$ DCs, or $CD11b^+$ DCs among all groups. In contrast, hosts receiving *Aim2*$^{-/-}$ and *Aim2*$^{-/-}$*Cxcl10*$^{-/-}$ DC-gp100 showed a lower proportion of T reg cells and a higher proportion of $CD4^+$ Teffs compared with those receiving WT and *Aim2*$^{-/-}$*Ifnar*$^{-/-}$ DC-gp100, whereas there was no difference in the percentage of IFN-γ– or TNF-α–producing PMELs among all groups (Fig. 4, C and D; and Fig. S3 C). In addition, the PMEL/T reg cell ratio was higher in hosts receiving *Aim2*$^{-/-}$ DC-gp100 than in those receiving WT and *Aim2*$^{-/-}$*Ifnar*$^{-/-}$ DC-gp100 (Fig. 4 C). Within the spleen, hosts receiving *Aim2*$^{-/-}$ DC-gp100 showed

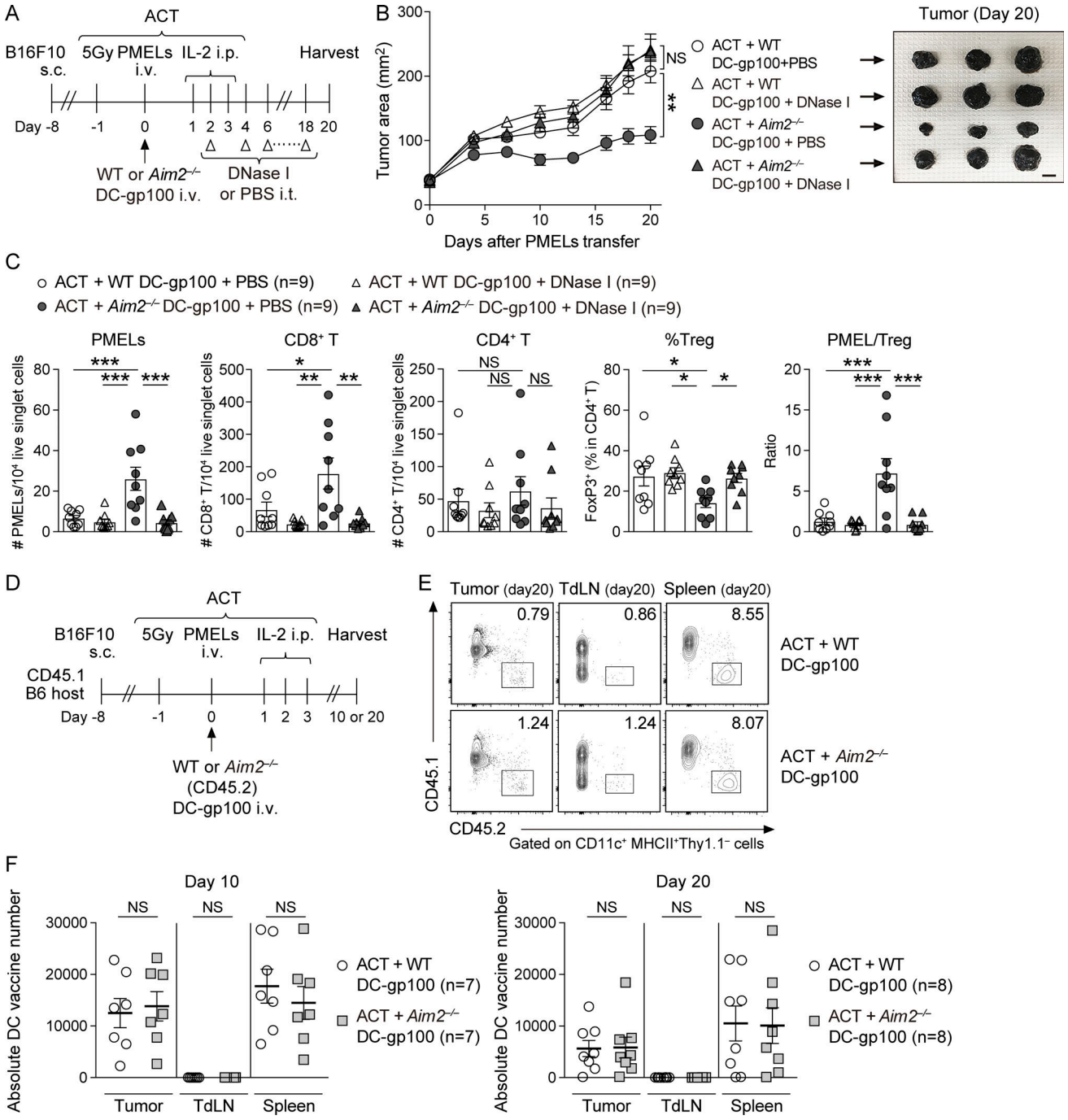

Figure 3. **Enhanced anti-melanoma immunity of vaccination with AIM2-deficient DCs is dependent on the recognition of tumor-derived DNA and independent of prolonged cell survival of vaccinated DCs. (A–C)** B16F10 mice were treated with ACT + WT or *Aim2*$^{-/-}$ DC-gp100 and intratumoral (i.t.) administration of DNase I or PBS. On day 20 after PMEL transfer, tissues were harvested. **(A)** Therapy regimen scheme. **(B)** Tumor growth over time (left; n = 9). Sample photo of B16F10 tumor on day 20 after PMELs transfer (right). Scale bar, 10 mm. **(C)** Flow cytometry analysis of the numbers of PMELs, CD8$^+$ T cells, and CD4$^+$ T cells among 10^4 live singlet cells, percentage of FoxP3$^+$ cells in CD4$^+$ T cells, and PMEL/T reg cell ratio in the tumor (n = 9). **(D)** Experimental scheme for analyzing DC vaccine infiltration in the tumor, TdLN, and spleen. B16F10-bearing CD45.1 congenic B6 mice were treated with ACT using 1.0 × 10^6 PMELs (CD45.2) + 1.0 × 10^6 WT or *Aim2*$^{-/-}$ DC-gp100 (CD45.2), and tissues were harvested on day 10 (n = 7) and day 20 (n = 8) after PMELs transfer. **(E)** Representative contour plot for CD45.2$^+$ Thy1.1$^-$CD11c$^+$ MHC-II$^+$ DC-gp100 (DC vaccine) present at the tumor, TdLN, and spleen on day 20 after PMELs transfer. **(F)** The absolute number of vaccinated DCs present in the tumor, TdLN, and spleen on days 10 (n = 7) and 20 (n = 8) after PMELs transfer. Data are shown as mean ± SEM and are pooled from four (B and C) or three (F) independent experiments or are representative of three independent experiments (E). *, P < 0.05; **, P < 0.01; ***, P < 0.001; two-way ANOVA with Tukey's multiple-comparisons test (B), one-way ANOVA with Tukey's multiple-comparisons test (C), or Mann–Whitney test (F).

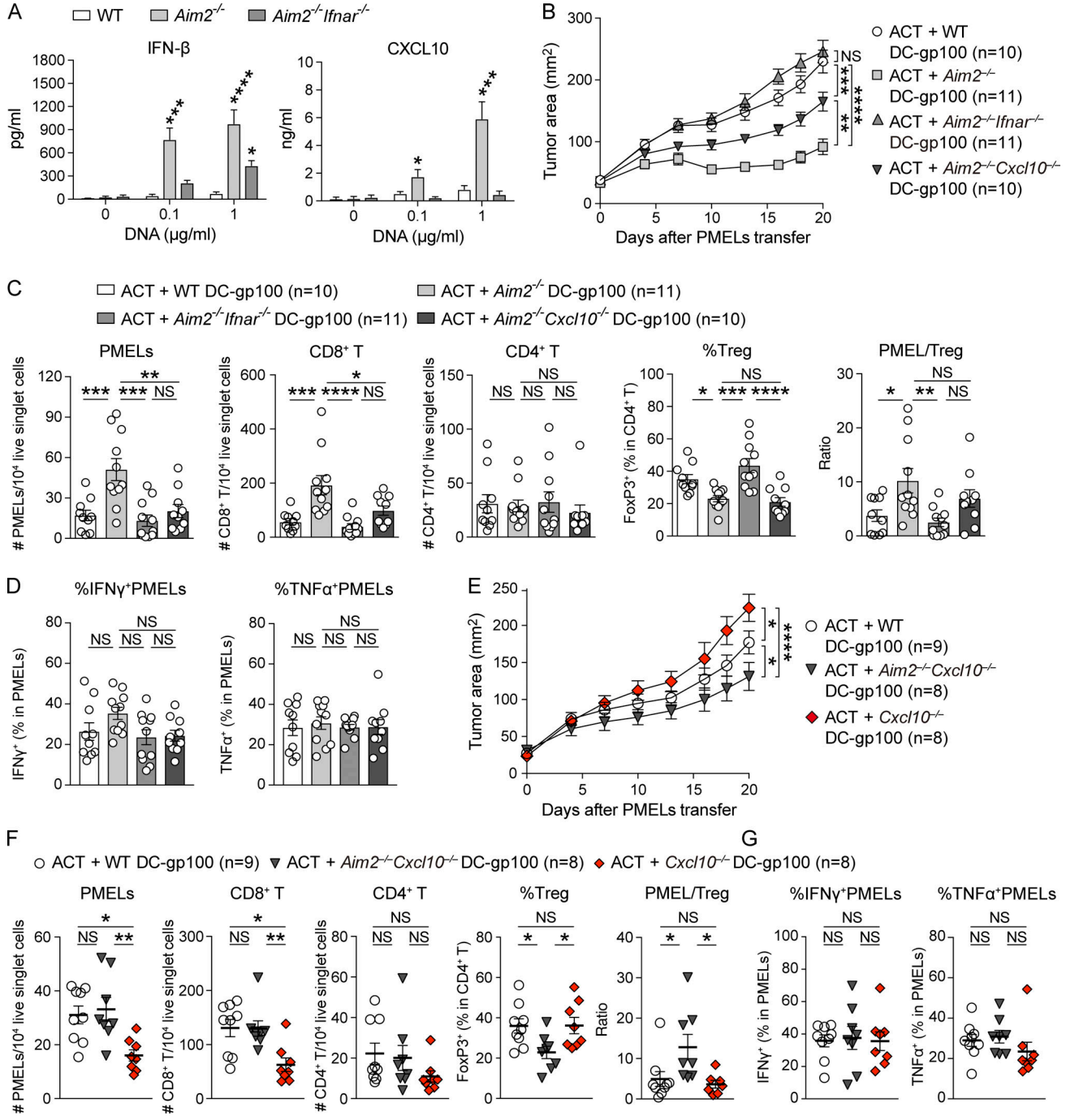

Figure 4. **AIM2-deficient DC vaccination facilitates tumor antigen–specific CD8⁺ T cell infiltration into the tumor via IFNAR signaling and CXCL10 production. (A)** IFN-β or CXCL10 in the supernatants of indicated BMDCs stimulated with 0, 0.1, or 1 μg/ml B16F10 DNA for 4 (IFN-β) or 10 h (CXCL10; *n* = 3). **(B–D)** B16F10 mice were treated with ACT + WT, *Aim2*$^{-/-}$, *Aim2*$^{-/-}$*Ifnar*$^{-/-}$, or *Aim2*$^{-/-}$*Cxcl10*$^{-/-}$ DC-gp100. On day 20 after PMELs transfer, tissues were harvested (*n* = 10 or 11). **(B)** Tumor growth over time. **(C and D)** Flow cytometry analysis of TILs. **(C)** The numbers of PMELs, CD8⁺ T cells, and CD4⁺ T cells among 10^4 live singlet cells, percentages of FoxP3⁺ cells in CD4⁺ T cells, and PMEL/T reg cell ratio. **(D)** The percentages of IFN-γ⁺ and TNF-α⁺ in CD8⁺ T cells. **(E–G)** Similar analysis as in B–D was performed on B16F10 mice treated by ACT with WT, *Aim2*$^{-/-}$*Cxcl10*$^{-/-}$, or *Cxcl10*$^{-/-}$ DC-gp100 (*n* = 8 or 9). Data are shown as mean ± SEM and are pooled from three independent experiments (A–G). *, P < 0.05; **, P < 0.01; ***, P < 0.001; ****, P < 0.0001; two-way ANOVA with Tukey's multiple-comparisons test (B and E) or one-way ANOVA with Dunnett's (A) or Tukey's (C, D, and F) multiple-comparisons test.

higher numbers of PMELs and CD8⁺ T cells than those receiving WT and *Aim2*$^{-/-}$*Ifnar*$^{-/-}$ DC-gp100, whereas there was no difference among all groups in TdLNs (Fig. S3 D). Moreover, there was no difference in the number of CD4⁺ T cells and proportion of T reg cells in TdLN and spleen among all groups (Fig. S3 E). These results suggest that *Aim2*$^{-/-}$ DCs during vaccination represent the primary type I IFN–sensing cells and that i.v. injection of the *Aim2*$^{-/-}$ DC vaccine promotes the migration of

antigen-specific CD8+ T cells into the tumor via CXCL10. In addition, tumor-infiltrating *Aim2*$^{-/-}$ DCs decrease T reg cell migration to the tumor through type I IFN signaling, but not via CXCL10.

To further examine whether the infiltration of PMELs into the tumor by *Aim2*$^{-/-}$ DCs was due to an increase of CXCL10 production, we performed ACT with WT, *Aim2*$^{-/-}$*Cxcl10*$^{-/-}$, or *Cxcl10*$^{-/-}$ DC-gp100. Among hosts receiving ACT with DC-gp100, those receiving *Cxcl10*$^{-/-}$ DC-gp100 exhibited the highest tumor burden, followed in order by WT and *Aim2*$^{-/-}$*Cxcl10*$^{-/-}$ DC-gp100 (Fig. 4 E). Within the tumor, hosts receiving *Cxcl10*$^{-/-}$ DC-gp100 had lower numbers of PMELs and CD8+ T cells than other groups. In contrast, hosts receiving *Aim2*$^{-/-}$*Cxcl10*$^{-/-}$ DC-gp100 had a similar number of PMELs and CD8+ T cells as hosts receiving WT DC-gp100 and showed a lower frequency of T reg cell and higher PMEL/T reg cell ratio than the other groups. Furthermore, there were no differences in number of CD4+ T cells or percentages of IFN-γ– or TNF-α–producing PMELs among all groups (Fig. 4, F and G). Collectively, these findings indicate that CXCL10 production is important for *Aim2*$^{-/-}$ DC-gp100 to recruit CD8+ T cells in the tumor and that *Aim2*$^{-/-}$ DC-gp100 exerts different mechanisms other than STING–type I IFN signaling to promote CD8+ T cells and suppress T reg cell migration into the tumor.

AIM2 is required for IL-1β and IL-18 production, which promotes melanoma T reg cell accumulation and tumor growth in vivo

Consistent with the well-established role of AIM2 as a caspase-1–activating inflammasome (Rathinam et al., 2010), AIM2 was required for the secretion of IL-1β and IL-18 from BMDCs in response to stimulation with tumor-derived DNA. The double-stranded DNA–induced IFN-β or CXCL10 production was normal in BMDCs lacking IL-1β or IL-18 as expected, suggesting that neither IL-1β nor IL-18 deficiency recapitulates the enhanced effect on the STING pathway seen with *Aim2*$^{-/-}$ BMDCs (Fig. 5 A). We next assessed whether there is an enhanced anti-tumor effect of DC vaccination by performing ACT with *Il1β*$^{-/-}$ or *Il18*$^{-/-}$ DC-gp100.

In hosts receiving WT, *Aim2*$^{-/-}$, or *Il1β*$^{-/-}$ DC-gp100, the tumor burden of those receiving *Il1β*$^{-/-}$ DC-gp100 was intermediate between those receiving WT and *Aim2*$^{-/-}$ DC-gp100 (Fig. 5 B). Within the tumor, hosts receiving *Aim2*$^{-/-}$ DC-gp100 had a greater number of PMELs and higher PMEL/T reg cell ratio than the other groups, and hosts receiving *Aim2*$^{-/-}$ DC-gp100 showed a greater number of CD8+ T cells than hosts receiving WT DC-gp100 (Fig. 5, C and D). Hosts receiving *Il1β*$^{-/-}$ DC-gp100 also showed a greater number of CD8+ T cells than hosts receiving WT DC-gp100 (Fig. 5 C). In contrast, hosts receiving *Aim2*$^{-/-}$and *Il1β*$^{-/-}$ DC-gp100 showed a lower proportion of T reg cells and a higher proportion of CD4+ Teffs than hosts receiving WT DC-gp100, while there was no difference in the numbers of CD4+ T cells, CD103+ DCs, or CD11b+DCs or percentages of IFN-γ– or TNF-α–producing PMELs among all groups (Fig. 5, D and E; and Fig. S4 A). Within the spleen, hosts receiving *Aim2*$^{-/-}$ DC-gp100 showed higher numbers of PMELs and CD8+ T cells than other groups, whereas there was no difference among all groups in TdLNs (Fig. S4 B). The numbers of CD4+ T cells or proportion of T reg cells in TdLN and spleen were similar among all groups (Fig. S4 C). Together, these data indicate that reduced production of IL-1β in *Aim2*$^{-/-}$ DC vaccine prevents T reg cell tumor infiltration and promotes anti-tumor immune responses, but this does not fully recapitulate the anti-tumor effect of AIM2 deficiency.

Similarly, in ACT with WT, *Aim2*$^{-/-}$, or *Il18*$^{-/-}$ DC-gp100, the tumor burden of hosts receiving *Il18*$^{-/-}$ DC-gp100 was intermediate between those receiving WT and *Aim2*$^{-/-}$ DC-gp100 (Fig. 5 F). Within the tumor, hosts receiving *Aim2*$^{-/-}$ DC-gp100 had a greater number of PMELs than other groups and a greater number of CD8+ T cells and higher PMEL/T reg cell ratio than hosts receiving WT but not *Il18*$^{-/-}$ DC-gp100 (Fig. 5, G and H). In contrast, hosts receiving *Aim2*$^{-/-}$ and *Il18*$^{-/-}$ DC-gp100 showed a lower proportion of T reg cells and a higher proportion of CD4+ Teffs than hosts receiving WT DC-gp100, while there was no difference in the numbers of CD4+ T cells, CD103+ DCs, or CD11b+ DCs or percentages of IFN-γ– or TNF-α–producing PMELs among all groups (Fig. 5, H and I; and Fig. S4 D). Within the spleen, hosts receiving *Aim2*$^{-/-}$ DC-gp100 showed higher numbers of PMELs than other groups, whereas there was no difference among all groups in TdLNs (Fig. S4 E). There was also no difference in CD8+ or CD4+ T cell number or proportion of T reg cells in TdLN and spleen among all groups (Fig. S4, E and F). These results suggest that reduced production of IL-18 in *Aim2*$^{-/-}$ DC vaccine could also prevent T reg cell tumor infiltration. Taken together, these findings reveal that AIM2 regulates anti-melanoma immunity of tumor-infiltrating DC vaccination both by suppressing the STING–type I IFN pathway and through its effects promoting IL-1β and IL-18 production in response to tumor-derived DNA.

Silencing AIM2 in vaccinated DCs enhances the efficacy of ACT against melanoma

To determine whether targeting AIM2 in the DC vaccine could be used therapeutically, we next evaluated whether silencing AIM2 expression could improve the efficacy of ACT in the setting of WT DC vaccination. We synthesized *Aim2*-targeting, hydrophobically modified, fully chemically stabilized siRNAs (*Aim2* siRNA-1 and *Aim2* siRNA-2), which have an ability to maintain sustained silencing with a single treatment (Hassler et al., 2018), to develop an AIM2-silenced DC vaccine. WT BMDCs transfected with *Aim2* siRNA (-1 or -2) showed markedly lower mRNA and protein expression of AIM2 than control siRNA–transfected and mock (transfection reagent only)-transfected BMDCs (Fig. 6, A and B). Furthermore, we observed that knockdown of *Aim2* mRNA persisted for as long as 22 d after transfection (Fig. 6 B).

Following ACT with DC-gp100 transfected with either control or *Aim2* siRNA (Fig. 6 C), we found that the tumor burden of hosts receiving *Aim2* siRNA–transfected DC-gp100 was smaller than those treated with control siRNA–transfected DC-gp100 (Fig. 6 D). Within the tumor, hosts receiving *Aim2* siRNA–transfected DC-gp100 had higher numbers of PMELs and CD8+ T cells, a higher proportion of CD4+ Teffs, a higher PMEL/T reg cell ratio, and a lower proportion of T reg cells than hosts with control siRNA–transfected DC-gp100, whereas there was no

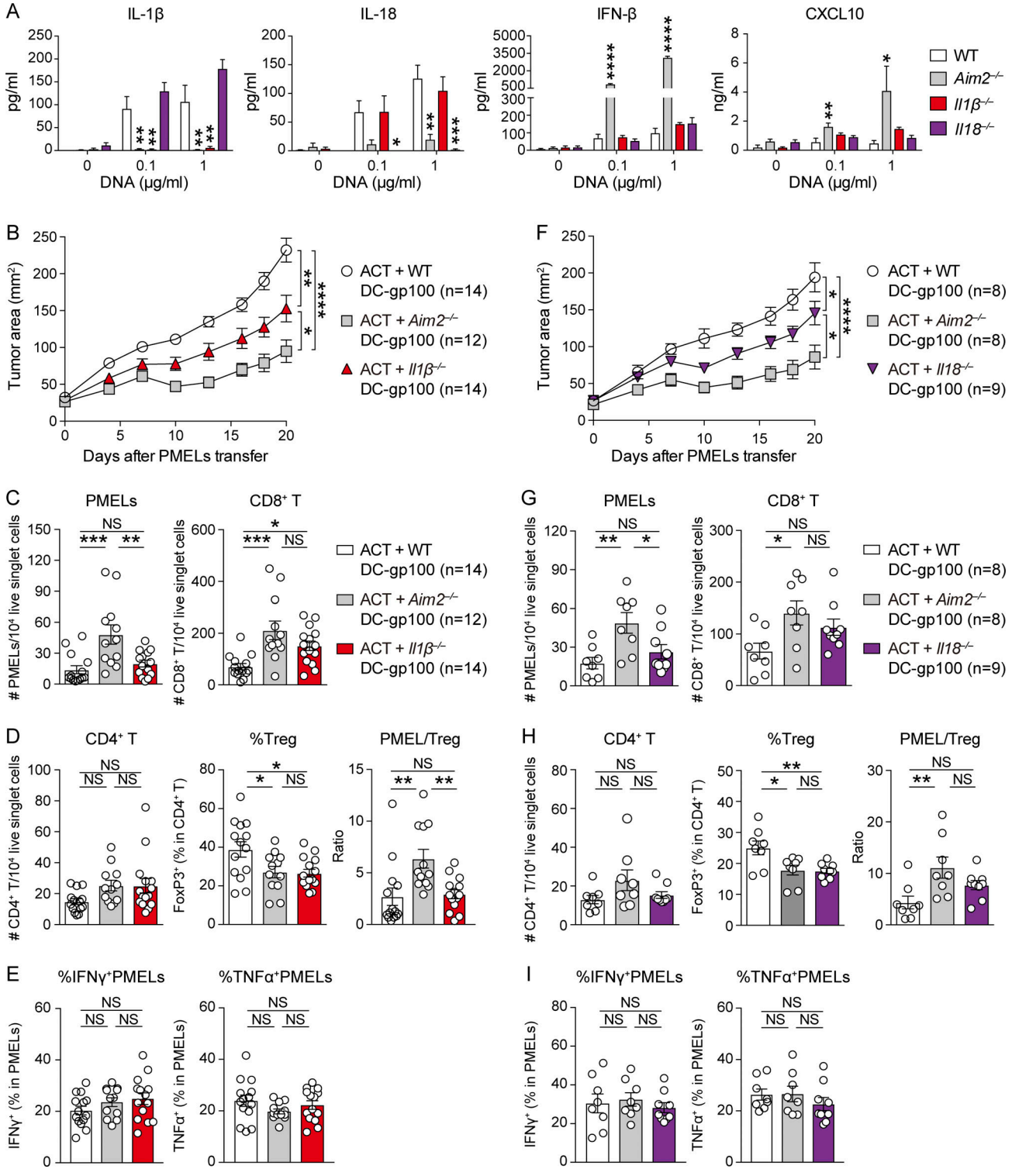

Figure 5. **Reduced IL-1β and IL-18 production by AIM2-deficient DC vaccination restricts T reg cell infiltration into the tumor. (A)** IL-1β, IL-18, IFN-β, and CXCL10 in the supernatants of indicated BMDCs stimulated with 0, 0.1, or 1 μg/ml B16F10 DNA for 4 (IFN-β) or 10 h (IL-1β, IL-18, and CXCL10; *n* = 3). **(B–E)** B16F10 mice were treated with ACT + WT, *Aim2*$^{-/-}$, or *Il1β*$^{-/-}$ DC-gp100. On day 20 after PMELs transfer, tissues were harvested (*n* = 12–14). **(B)** Tumor growth over time. **(C–E)** Flow cytometry analysis of TILs. The numbers of PMELs, CD8$^+$ T cells (C), and CD4$^+$ T cells among 10^4 live singlet cells, percentage of FoxP3$^+$ cells in CD4$^+$ T cells, PMEL/T reg ratio (D), and the percentages of IFN-γ$^+$ and TNF-α$^+$ (E) in CD8$^+$ T cells. **(F–I)** B16F10 mice were treated with ACT + WT, *Aim2*$^{-/-}$, or *Il18*$^{-/-}$ DC-gp100. On day 20 after PMELs transfer, tissues were harvested (*n* = 8 or 9), and similar analysis as in B–E was performed. Data are shown as mean ± SEM and are pooled from three independent experiments (A–I). *, P < 0.05; **, P < 0.01; ***, P < 0.001; ****, P < 0.0001; two-way ANOVA with Tukey's multiple-comparisons test (B and F) or one-way ANOVA with Dunnett's (A) or Tukey's (C–E and G–I) multiple-comparisons test.

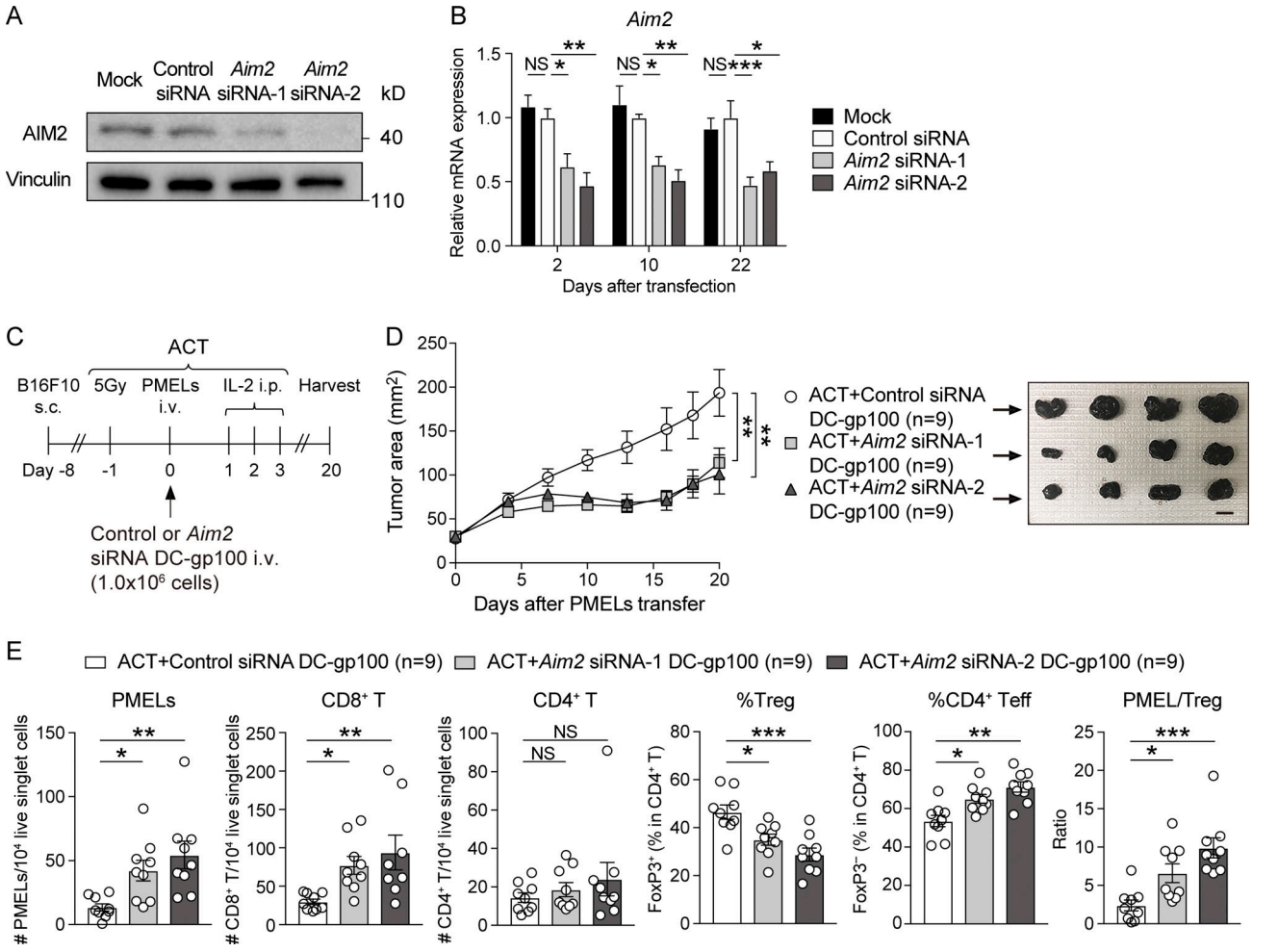

Figure 6. **AIM2-silenced DC vaccine improves the efficacy of ACT against melanoma. (A)** Immunoblotting for AIM2 and vinculin in the lysates of mock-, control siRNA–, or *Aim2* siRNA– (-1 or -2) transfected WT BMDCs 48 h after transfection. **(B)** Quantitative RT-PCR analysis of the *Aim2* mRNA expression in mock-, control siRNA–, or *Aim2* siRNA–transfected WT BMDCs 2, 10, and 22 d after transfection (n = 6). **(C–E)** B16F10 mice were treated with ACT + control siRNA– or *Aim2* siRNA–transfected WT DC-gp100. On day 20 after PMELs transfer, tissues were harvested. **(C)** Therapy regimen scheme. **(D)** Tumor growth over time (left; n = 9). Sample photo of B16F10 tumor on day 20 after PMELs transfer (right). Scale bar, 10 mm. **(E)** Flow cytometry analysis of the numbers of PMELs, CD8⁺, and CD4⁺ T cells among 10^4 live singlet cells, percentage of FoxP3⁺ cells in CD4⁺ T cells, and PMEL/T reg cell ratio in the tumor (n = 9). Data are shown as mean ± SEM and are representative of three independent experiments (A) or are pooled from two independent experiments (B, D, and E). *, P < 0.05; **, P < 0.01; ***, P < 0.001; two-way ANOVA with Tukey's multiple-comparisons test (D) or one-way ANOVA with Dunnett's multiple-comparisons test (B and E).

difference in the numbers of CD4⁺ T cells (Fig. 6 E). Furthermore, the number of PMELs in the spleen was higher in hosts receiving *Aim2* siRNA–transfected DC-gp100 than in hosts with control siRNA–transfected DC-gp100, whereas it did not differ in TdLNs. Furthermore, there was no difference in the numbers of CD8⁺ or CD4⁺ T cells or proportion of T reg cells in TdLN and spleen (Fig. S4 G). These results indicate that treatment of WT DCs with *Aim2* siRNAs before vaccination recapitulates the therapeutic benefit observed with *Aim2*$^{-/-}$ DC vaccine, providing a therapeutic option relevant to clinical care.

AIM2-deficient DC vaccination provides additive anti-tumor effects when combined with anti–PD-1 immunotherapy

Because the failure of immunotherapy with PD-1 Ab is frequently due to cold tumors without sufficient T cell infiltration and following our observation that *Aim2*$^{-/-}$ DC vaccination enhances tumor infiltration, we assessed whether *Aim2*$^{-/-}$ DC-gp100 could augment the efficacy of anti–PD-1 immunotherapy in this poorly immunogenic B16F10 melanoma model. To do this, we treated B16F10 mice with control IgG, PD-1 Ab, WT DC-gp100, *Aim2*$^{-/-}$ DC-gp100, PD-1 Ab + WT DC-gp100, or PD-1 Ab + *Aim2*$^{-/-}$ DC-gp100 (Fig. 7 A). Compared with hosts treated with control IgG, only hosts that received PD-1 Ab + *Aim2*$^{-/-}$ DC-gp100 showed lower tumor burden (Fig. 7 B). Notably, the tumor burden of hosts treated with *Aim2*$^{-/-}$ DC-gp100 was similar to that of hosts treated with WT DC-gp100, unlike previous experiments in which we used radiation as part of ACT, whereas hosts treated with PD-1 Ab + *Aim2*$^{-/-}$ DC-gp100 showed lower tumor burden than hosts treated with PD-1 Ab + WT DC-gp100 (Fig. 7 B). These results imply that i.v. injection of *Aim2*$^{-/-}$ DC vaccine without radiation does not provide enough release of tumor-derived DNA by itself and requires cotreatment such as

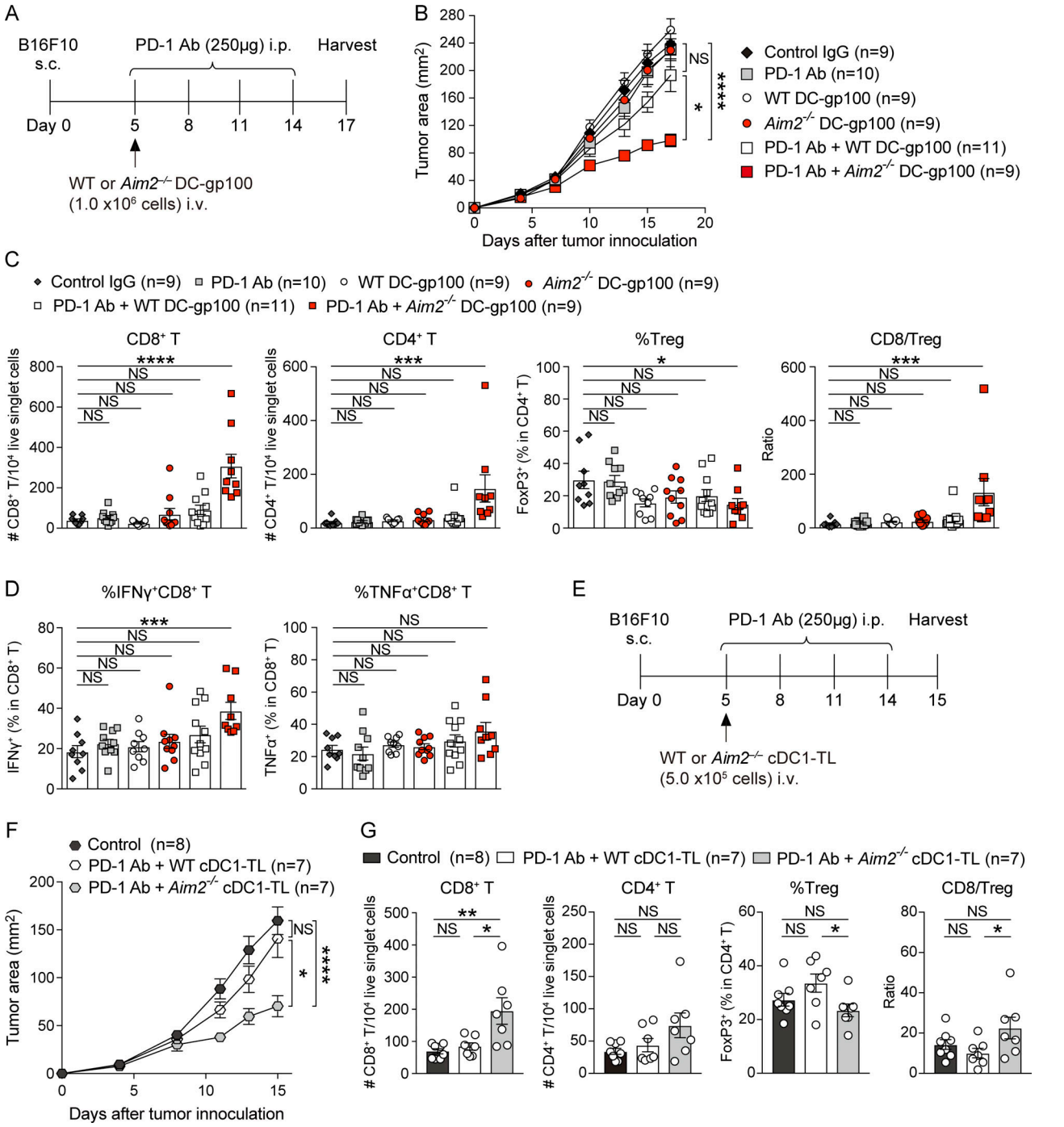

Figure 7. **AIM2-deficient DC vaccination potentiates the efficacy of anti–PD-1 immunotherapy. (A–D)** WT mice were inoculated s.c. with 1.0 × 10^6 B16F10 cells on day 0 and treated from the indicated time points by treatments. On day 17, tissues were harvested. **(A)** Therapy regimen scheme. **(B)** Tumor growth over time (n = 9–11). **(C and D)** Flow cytometry analysis of TILs (n = 9–11). **(C)** The numbers of CD8⁺ and CD4⁺ T cells among 10^4 live singlet cells, percentage of FoxP3⁺ cells in CD4⁺ T cells, and CD8/T reg cell ratio. **(D)** The percentages of IFN-γ⁺ and TNF-α⁺ in CD8⁺ T cells. **(E–G)** WT mice were inoculated s.c. with 1.0 × 10^6 B16F10 cells on day 0 and treated from the indicated time points by PBS (control), WT cDC1-TL + PD-1 Ab, or *Aim2*$^{-/-}$ cDC1-TL + PD-1 Ab. On day 15, tissues were harvested. **(E)** Therapeutic regimen. **(F)** Tumor growth over time (n = 7 or 8). **(G)** Flow cytometry analysis of the numbers of CD8⁺ and CD4⁺ T cells among 10^4 live singlet cells, percentage of FoxP3⁺ cells in CD4⁺ T cells, and CD8/T reg cell ratio in the tumor (n = 7 or 8). Data are shown as mean ± SEM and are pooled from three (B–D) or two (F and G) independent experiments. *, P < 0.05; **, P < 0.01; ***, P < 0.001; ****, P < 0.0001; two-way ANOVA with Tukey's multiple-comparisons test (B and F) or one-way ANOVA with Dunnett's (C and D) or Tukey's (G) multiple-comparisons test.

ACT or PD-1 Ab to enhance anti-melanoma immunity. Hosts receiving PD-1 Ab + *Aim2*$^{-/-}$ DC-gp100 were the only group that showed greater numbers of CD8$^+$ and CD4$^+$ T cells, higher CD8/T reg cell ratio, and percentage of IFN-γ–producing CD8$^+$ T cells, as well as lower proportion of T reg cells and higher proportion of CD4$^+$ Teffs compared with the control group (Fig. 7, C and D; and Fig. S5 A). In contrast, there were no differences in the numbers of CD103$^+$ or CD11b$^+$ DCs or percentage of TNF-α–producing CD8$^+$ T cells in the tumor as well as total CD8$^+$ T or CD4$^+$ T cells, proportion of T reg cells, or CD8/T reg cell ratio in the TdLNs or spleen among all treatments (Fig. 7 D; and Fig. S5, B–D). Thus, these results demonstrate that *Aim2*$^{-/-}$ DC vaccination provides additive anti-melanoma immunity not only to ACT but also to anti–PD-1 immunotherapy.

To date, MoDCs generated from CD14$^+$ blood monocytes via treatment with GM-CSF and IL-4 have been primarily used for DC vaccines in clinical trials for cancers. However, they present limited efficacy (Anguille et al., 2014), in part due to reduced migration and T cell priming capacity relative to natural DC subsets (Perez and De Palma, 2019; Zhou et al., 2020). Indeed, recent transcriptome and mass cytometry analyses revealed that MoDCs are phenotypically different and do not overlap with any DC subset localized in human tissues (Alcántara-Hernández et al., 2017; Villani et al., 2017). Thus, naturally occurring DC subsets have been the focus for next-generation DC vaccines, and they show promise in initial studies of tumor immunotherapy (Garg et al., 2017). Furthermore, a number of clinical trials demonstrated that DC vaccines pulsed with tumor-associated antigen peptides exhibit lower overall response than DC vaccines loaded with whole tumor lysate, which encompasses a broader tumor antigen repertoire (Neller et al., 2008).

To provide data more relevant to current clinical studies, we sought to replicate our findings using conventional type 1 DCs (cDC1s), a naturally occurring DC subset that has strong capacity to induce CD8$^+$ T cell responses (Wculek et al., 2020), and performed anti–PD-1 immunotherapy with *Aim2*$^{-/-}$ tumor lysate–loaded cDC1 vaccine (cDC1-TL). Similar to *Aim2*$^{-/-}$ DC-gp100, hosts treated with PD-1 Ab + *Aim2*$^{-/-}$ cDC1-TL showed lower tumor burden than hosts treated with PBS (control) or PD-1 Ab + WT DC cDC1-TL (Fig. 7, E and F). Within the tumor, hosts receiving PD-1 Ab + *Aim2*$^{-/-}$ cDC1-TL showed a greater number of CD8$^+$ T cells, higher CD8/T reg cell ratio, a lower proportion of T reg cells, and a higher proportion of CD4$^+$ Teffs compared with hosts receiving PD-1 Ab + WT cDC1-TL, whereas there were no differences in numbers of CD8$^+$ T cells, CD103$^+$ DCs, or CD11b$^+$ DCs or percentages of IFN-γ– or TNF-α–producing CD8$^+$ T cells among all groups (Fig. 7 G; and Fig. S5, E and F). These results demonstrate that the enhanced anti-tumor immunity effect by targeting AIM2 can be translated not only to peptide-pulsed BMDCs but also to tumor lysate–loaded naturally occurring DCs, which are more clinically relevant DC vaccines that have a potential to induce stronger anti-tumor immunity than peptide-pulsed MoDCs.

siRNA targeting of AIM2 in human monocyte–derived DCs results in enhanced responses to tumor-derived DNA

Finally, we addressed whether the therapeutic implications in our mouse model could be extended to the human system. First, we confirmed that AIM2 protein is expressed in mature human MoDCs. In addition, this expression could be effectively silenced by *AIM2* siRNA (-1 or -2; Fig. 8 A). In contrast to mouse BMDCs that express the cDC2 marker CD11b (Fig. S2 F; Mayer et al., 2014), the LPS-primed siRNA-transfected human MoDCs all adhered to the culture dish during transfection and expressed the cDC1 marker CD141, while few expressed the cDC2 marker CD1c, consistent with an earlier observation (Fig. 8 B; Kim et al., 2019). Furthermore, we found that priming with LPS to convert immature MoDCs to mature MoDCs induces AIM2 expression further (Fig. 8 C). Next, we tested whether AIM2 in mature MoDCs inhibits the activation of STING–type I IFN signaling and promotes the secretion of IL-1β and IL-18 in response to cytosolic tumor-derived DNA as we observed in mouse BMDCs. We stimulated LPS-primed MoDCs with human melanoma xenograft-derived DNA (melanoma DNA), delivered via lipofection. IRF3 is a protein activated by STING–type I IFN signaling. We found that LPS priming of MoDCs induced pTBK1 regardless of stimulation by melanoma DNA, and *AIM2* siRNA–transfected MoDCs showed similar levels of pTBK1 in response to exposure to melanoma DNA compared with control siRNA-transfected MoDCs. In contrast, *AIM2* siRNA–transfected MoDCs showed enhanced pIRF3 in response to exposure to melanoma DNA compared with control siRNA–transfected MoDCs (Fig. 8 D). Furthermore, *AIM2* siRNA–transfected and control siRNA–transfected MoDCs induced IFN-β, CXCL10, IL-1β, and IL-18 production following stimulation with melanoma DNA, and *AIM2* siRNA–transfected MoDCs secreted more IFN-β and CXCL10 (Fig. 8 E) but less IL-1β and IL-18 than control siRNA–transfected MoDCs (Fig. 8 F).

Since it was recently reported that DNA-triggered IL-1β and IL-18 production depends on the NLRP3 in human monocytes (Gaidt et al., 2017), we determined whether IL-1β and IL-18 production in response to DNA could be suppressed by the NLRP3 inhibitor MCC950 in human MoDCs. We found that MCC950 treatment had no impact on DNA-triggered IL-1β and IL-18 production of control siRNA– and *AIM2* siRNA–transfected MoDCs (Fig. 8 G). These results imply that AIM2 in human mature MoDCs responds in a similar way to mouse BMDCs and thus can be used to generate a DC vaccine to improve the efficacy of melanoma immunotherapy in patients.

Discussion

Existing immunotherapies for melanoma have limited efficacy when the tumor lacks sufficient infiltration by CD8$^+$ T cells, a condition known as a cold tumor. Here, we reveal that vaccination using *Aim2*$^{-/-}$ BMDCs provides an alternate approach to enhance immunotherapy, which may achieve therapeutic efficacy even for patients with cold tumors. Consistent with previous reports using WT DCs (Krzastek et al., 2018; Lou et al., 2004; Mullins et al., 2003), we found that vaccinated *Aim2*$^{-/-}$ DCs home directly to the tumor, TdLN, and spleen. We determined that vaccinated *Aim2*$^{-/-}$ BMDCs in the spleen promote T cell proliferation and that vaccinated *Aim2*$^{-/-}$ BMDCs in the tumor facilitate T cell recruitment into the tumor through the production of CXCL10. They also diminish T reg cell recruitment

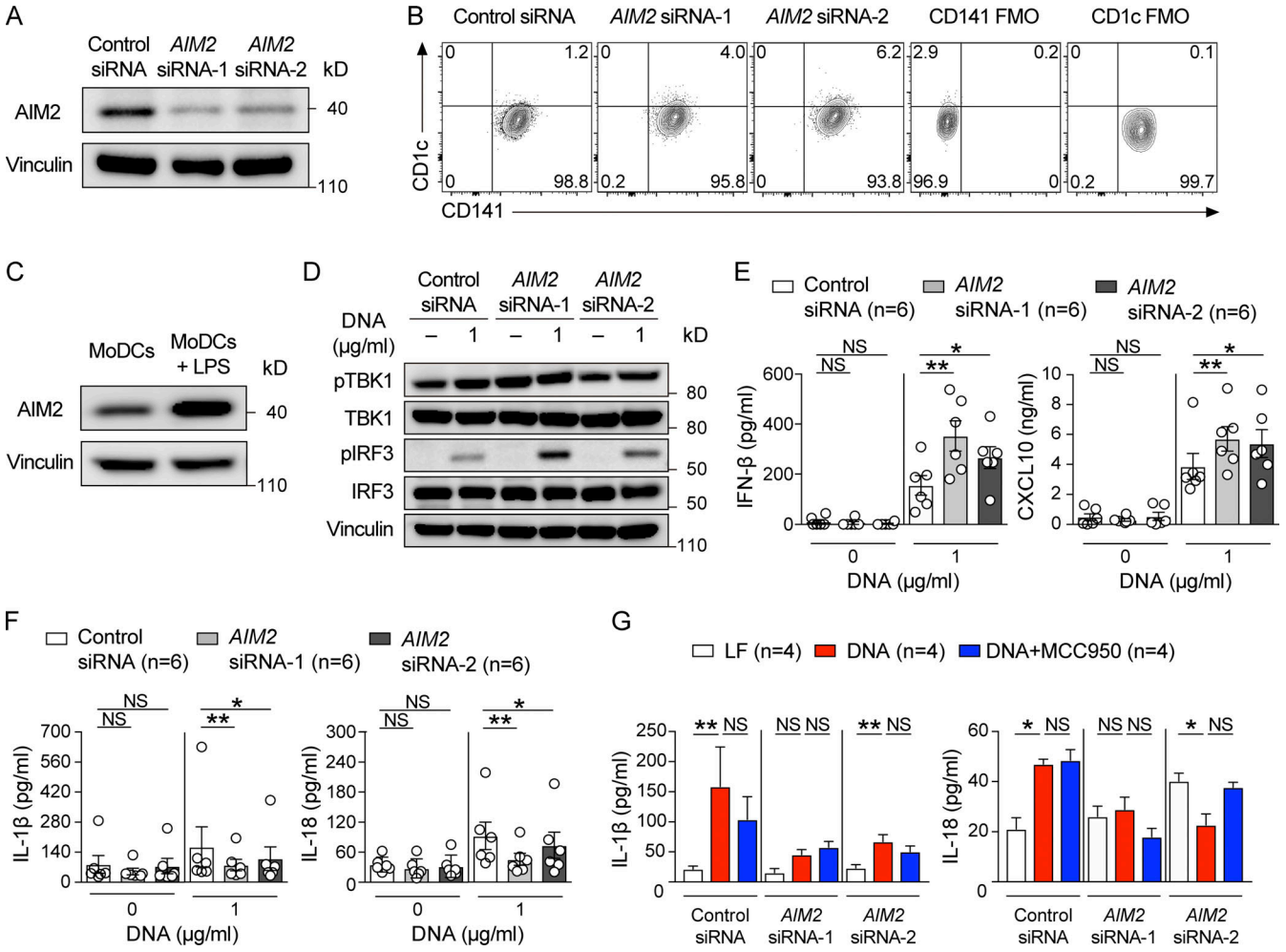

Figure 8. **siRNA targeting of AIM2 in human MoDCs results in increased activation similar to mouse BMDCs. (A)** Immunoblotting for AIM2 and vinculin in the lysates of control siRNA– or *AIM2* siRNA (-1 or -2)–transfected LPS-primed human MoDCs 48 h after transfection. **(B)** Flow cytometry staining of CD141 and CD1c in control siRNA– or *AIM2* siRNA–transfected LPS-primed human MoDCs. FMO, fluorescence minus one control. **(C)** Immunoblotting for AIM2 and vinculin in the lysates of non– or LPS-primed human MoDCs. **(D)** Immunoblotting for pTBK1, TBK1, pIRF3, IRF3, and vinculin in the lysates of indicated LPS-primed human MoDCs stimulated with 0 or 1 μg/ml human melanoma–derived DNA (DNA) for 8 h. IFN-β, CXCL10 (E), IL-1β, and IL-18 (F) in the supernatants of indicated LPS-primed human MoDCs stimulated with 0 or 1 μg/ml DNA for 12 h (n = 6). **(G)** IL-1β and IL-18 in the supernatants of indicated LPS-primed human MoDCs stimulated with Lipofectamine (LF; 1 μl/ml), DNA (1 μg/ml), or DNA (1 μg/ml) and MCC950 (1 μM) for 12 h (n = 4). Data are shown as mean ±SEM and are representative of three (A–F) or two (G) independent experiments. *, P < 0.05; **, P < 0.01; Friedman test with Dunn's multiple-comparisons test (E–G).

into the tumor, and both effects require autologous signaling by type I IFNs. This pathway may be partially responsible for therapeutic responses previously observed following therapeutic peritumoral and intratumoral injections of type I IFNs (Kakizaki et al., 2015; Lucarini et al., 2017).

It is not yet clear how vaccination with *Aim2*$^{-/-}$ DCs resulted in diminished T reg cell numbers within the tumor. We determined that this was not dependent on CXCL10 but may have been partially due to reduced IL-1β and IL-18 secretion, as DC vaccination with each cytokine knockout partially recapitulated this effect. IL-18 has been reported to drive T reg cell conversion in vivo (Oertli et al., 2012), but most studies suggest that IL-1β impairs T reg cell development and function (Brinster and Shevach, 2008; Pan et al., 2017). We found that this effect on T reg cells at least partially required autologous signaling through IFN-α/β receptor (IFNAR), as *Aim2*$^{-/-}$*Ifnar*$^{-/-}$ DC-gp100 lost this function. We also found that the amount of IFN-β was higher in the tumor and spleen of hosts receiving *Aim2*$^{-/-}$ DC-gp100 compared with hosts receiving WT DC-gp100, whereas there was no difference in the TdLNs between the two groups. The amount of IFN-β was highest in the tumor, followed in order by TdLN and then spleen. Based on these results, we speculate that there is a threshold needed for IFN-β to suppress T reg cell migration in the tissue and that the IFN-β protein level in the spleen was insufficient to suppress T reg cell migration into that location. In addition, it is likely that the lack of difference in IFN-β protein level in the TdLNs between the two groups was one of the reasons why there was no difference in the percentage of T reg cells at that location. Others have reported that APCs are the primary producers of CCL22, a cytokine that promotes T reg cell migration within the melanoma microenvironment. Peritumoral and intratumoral injection of type I IFN suppressed T reg

cell tumor migration by suppressing CCL22 production in tumor-infiltrating APCs (Anz et al., 2015; Kakizaki et al., 2015; Lucarini et al., 2017). Furthermore, type I IFN has been reported to directly inhibit proliferation of T reg cells (Pace et al., 2010; Srivastava et al., 2014). Thus, increased production of type I IFN by *Aim2*$^{-/-}$ DC-gp100 may have resulted in similar effects.

Like cGAS, AIM2 is a cytosolic DNA sensor, but in contrast to inducing type I IFN secretion after activation, AIM2 forms a caspase-1–activated inflammasome. Early studies in *Aim2*$^{-/-}$ mice showed that AIM2 also inhibits type I IFN production, which was recently shown to be due to limiting cGAS-STING signaling in vitro (Banerjee et al., 2018; Corrales et al., 2016; Rathinam et al., 2010). The primary function of the AIM2 inflammasome is to control the proteolytic maturation of IL-1β and IL-18 and the pyroptosis effector molecule gasdermin D. The improved tumor responses following DC vaccination with *Aim2*$^{-/-}$ DCs are due at least in part to enhanced STING activation and subsequent type I IFN signaling, as *Aim2*$^{-/-}$*Sting*$^{-/-}$ and *Aim2*$^{-/-}$*Ifnar*$^{-/-}$ DC-gp100 failed to exhibit this enhanced effect. We also found that *Aim2*$^{-/-}$*Cxcl10*$^{-/-}$ DC vaccination promotes stronger tumor responses than *Cxcl10*$^{-/-}$ DC vaccination by facilitating recruitment of CD8^{+} T cells and suppressing T reg cell migration. This indicates that *Aim2*$^{-/-}$ DC vaccines work through different pathways than STING–type I IFN signaling to facilitate CD8^{+} T cells and suppress T reg cell migration into the tumor. Indeed, and consistent with other studies, we found that DC-derived IL-1β and IL-18 promote tumor growth, as both *Il1β*$^{-/-}$ and *Il18*$^{-/-}$ DC-gp100 induce improved therapeutic responses. Furthermore, we examined whether delayed cell death of DC vaccines could be another reason for the therapeutic efficacy of vaccination with *Aim2*$^{-/-}$ DCs; however, this was unlikely due to a lack of survival advantage observed for DCs following transfer, as we observed an equal number of WT or *Aim2*$^{-/-}$ DCs in the tumor at multiple time points. Since it has been demonstrated by others that antigen-loaded DCs can be rapidly eliminated by antigen-specific CD8^{+} T cells via perforin in vivo (Yang et al., 2006), *Aim2*$^{-/-}$ DC-gp100 may have been eliminated by a similar mechanism, thereby showing similar numbers of TIDCs as hosts that received ACT with WT DC-gp100. Collectively, our data indicate that vaccination using *Aim2*$^{-/-}$ DCs may provide enhanced therapeutic responses compared with treating with STING agonists alone, since this approach both activates STING–type I IFN signaling and eliminates the pro-tumor effects of IL-1β and IL-18.

It was recently reported that IL-1β improves the efficacy of ACT by promoting PMEL migration into the tumor as well as the functionality of PMELs (Lee et al., 2019). A possible explanation for the discrepancy with our data may be that the authors administered IL-1β systemically, and in those cases IL-1β could signal the circulating PMELs or endothelial cells, whereas in our study, IL-1β was produced in the tumor microenvironment by vaccinated WT DCs, where many types of cells such as myeloid cells could be signaled by the cytokine. Consistent with this hypothesis, it was previously reported that Tet2, a DNA methylcytosine dioxygenase, is induced by the IL-1β–IL-1R–MyD88 axis in tumor-associated MACs and that myeloid-specific deletion of Tet2 suppressed T reg cell migration and CD8^{+} T cell infiltration, thereby suppressing the growth of YUMM1.7 melanoma growth in vivo (Pan et al., 2017). In addition, it was recently reported that anti–IL-1β Ab treatment prevents B16F10 melanoma growth in vivo in WT mice (Tian et al., 2020) by increasing the number of CD8^{+} T cells in the tumor, similar to our results. Thus, IL-1β signaling appears to induce cell type–specific responses and set the inflammatory tone of anti–tumor immunity in aggregate.

There has been some discussion about the role of the AIM2 inflammasome in human primary myeloid cells. AIM2 was dispensable for cytosolic DNA-mediated inflammasome activation in human primary monocytes and could be functionally replaced by cGAS-STING-NLRP3 activation alone during inflammasome activation by DNA (Gaidt et al., 2017). In contrast, the production of IL-1β and IL-18 was dependent on AIM2 in human monocyte-derived MACs, and AIM2 inhibition led to the enhanced activation of IFN-β production following stimulation with cytosolic DNA (Wang et al., 2018). Thus, we examined the function of AIM2 in human MoDCs, which revealed that the ability of AIM2 to antagonize STING as well as produce IL-1β and IL-18 was conserved in human MoDCs as monocyte-derived MACs. These data support the hypothesis that the enhanced anti-melanoma immunity of *Aim2*$^{-/-}$ DC vaccination observed in the melanoma mouse model could be extended to human MoDCs transfected with *AIM2* siRNA.

Our data support using vaccination with *Aim2*$^{-/-}$ DCs as an adjuvant to ACT therapy or treatment with PD-1 Abs. In humans, this approach would require the generation of MoDCs from peripheral blood mononuclear cells (PBMCs), pretreatment with *AIM2* siRNA, and then transfer into the patient i.v. or by injection directly into the tumor. Our observation that *AIM2* siRNA–transfected human MoDCs exhibited enhanced responses to tumor-derived DNA, similar to mouse BMDCs, supports this hypothesis. Irradiation was required for responses using DC vaccination and ACT alone. This is presumably through cellular damage to the tumor and subsequent release of DNA to activate STING, as intratumoral injection of DNase I eliminated the effect. This is consistent with previous studies reporting that radiation therapy activates STING–type I IFN signaling on TIDCs (Deng et al., 2014; Hou et al., 2018). However, when combined with PD-1 Ab treatment, DC vaccination was sufficient to induce anti-tumor responses without the need for concomitant irradiation or ACT. In future studies, i.v. injection of DC-targeted, self-delivering *Aim2* siRNAs alone could prove to be sufficient for this effect, which would simplify the treatment regimen.

Materials and methods

Cell culture

The murine melanoma cell line B16F10 was obtained from American Type Culture Collection, the murine melanoma cell line B16-Flt3L was kindly provided by Dr. G. Dranoff (Harvard University, Cambridge, MA), and the murine melanoma cell line YUMM1.7 was kindly provided by Dr. M. Bosenberg (Yale University, New Haven, CT; now available at American Type Culture Collection). B16F10 and B16-Flt3L were cultured in DMEM (Corning) supplemented with 10% FBS and 100 U/ml penicillin/

streptomycin (PS). YUMM1.7 cells were cultured in DMEM/F12 (Gibco) supplemented with 10% FBS, 100 U/ml PS (Corning), and 1% nonessential amino acids solution (Gibco). All cell lines included in the study were profiled at passage 4–9 to abrogate the heterogeneity introduced by long-term culture. All cell lines were routinely confirmed negative for *Mycoplasma* species by RAPIDMAP-21 (Taconic Biosciences) and were maintained at 37°C in a humidified atmosphere of 5% CO_2.

Mice

C57BL/6 (B6; CD45.2) WT, *Ifnar*$^{-/-}$, *Cxcl10*$^{-/-}$, *Il-18*$^{-/-}$, CD45.1 congenic B6, Thy1.1^{+} PMEL TCR transgenic, and NSG mice were obtained from The Jackson Laboratory. *Sting*$^{-/-}$ (Ishikawa and Barber, 2008) mice were kindly provided by Dr. D. Stetson (University of Washington, Seattle, WA) and *Il1β*$^{-/-}$ mice (Horai et al., 1998) were kindly provided by Dr. D. Golenbock (University of Massachusetts Medical School [UMMS], Worcester, MA), and these mice were backcrossed to C57BL/6 for more than 10 generations at the UMMS. *Aim2*$^{-/-}$ mice (Jones et al., 2010) of C57BL/6 background (Jones et al., 2010) were obtained from Genentech. *Aim2*$^{-/-}$ mice were intercrossed with *Sting*$^{-/-}$, *Ifnar*$^{-/-}$, or *Cxcl10*$^{-/-}$ mice to produce *Aim2*$^{-/-}$*Sting*$^{-/-}$, *Aim2*$^{-/-}$*Ifnar*$^{-/-}$, and *Aim2*$^{-/-}$*Cxcl10*$^{-/-}$ mice. Both male and female mice (aged 6–14 wk) were included in the experiments, with age- and sex-matched mice used throughout.

Generation of BMDCs and peptide-pulsed DC vaccine

BMDCs were generated in accordance with a modified version of a method described previously (Helft et al., 2015; Lou et al., 2004). Briefly, bone marrow cells isolated from the femurs and tibiae of 7–14-wk-old WT, *Aim2*$^{-/-}$, *Sting*$^{-/-}$, *Cxcl10*$^{-/-}$, *Aim2*$^{-/-}$*Sting*$^{-/-}$, *Aim2*$^{-/-}$*Ifnar*$^{-/-}$, *Aim2*$^{-/-}$*Cxcl10*$^{-/-}$, *Il1β*$^{-/-}$, and *Il-18*$^{-/-}$ mice were filtered through a 70-µm nylon strainer, and red blood cells were lysed by ammonium-chloride-potassium lysis buffer (Sigma Aldrich) and cultured in BMDC medium (RPMI-1640 containing 10% FBS, 100 U/ml PS, 2 mM L-glutamine [Gibco], 50 µM 2-mercaptoethanol [Sigma Aldrich], 20 ng/ml GM-CSF [PeproTech], and 10 ng/ml IL-4 [PeproTech]).

The BMDC medium was replaced on days 3 and 6. On day 8, nonadherent cells were harvested, washed two times with PBS, and used for in vitro experiments. DC purity was assessed by flow cytometry to ensure staining for markers CD11c, MHC II, CD11b, and CD86 on BMDCs. For the generation of peptide-pulsed DC vaccine (DC-gp100), nonadherent cells were pulsed for 3 h at 37°C in 5% CO_2 with 10 µM of the human $gp100_{25–33}$ (hgp100) peptide (GenScript) in Opti-MEM medium (Gibco) and washed three times with PBS before their use.

Generation of B16F10 tumor cell lysate and tumor lysate–loaded cDC1 vaccine

Tumor lysate and cDC1-TL were generated as described previously (Wculek et al., 2019). Briefly, B16F10 tumor cells were adjusted to 4 × 10^6 cells/ml in RPMI-1640 supplemented with 10% FBS, 2.0 ml per well plated in 6-well plates (Corning) and treated with 300 mJ/cm^2 UV irradiation using a Stratalinker UV Cross-linker 1800 (Stratagene). Cells were then cultured for 24 h at 37°C in 5% CO_2, subjected to three freeze (liquid nitrogen)/thaw (37°C) cycles of 30 min each, and passed through a 40-µm cell strainer before addition to purified CD8^{+} DCs.

To expand cDC1, 2.5 × 10^6 B16-Flt3L cells in 100 µl of PBS were implanted s.c. into the flanks of WT and *Aim2*$^{-/-}$ mice. On day 10 after injection, spleens were harvested and CD8^{+} DCs were enriched using the CD8^{+} DC isolation kit (Miltenyi Biotec). Purified CD8^{+} DCs were plated at a density of 1.0 × 10^6 cells/ml in BMDC medium with 20 µg/ml of poly I:C LMW (InVivoGen) and B16F10 tumor cell lysate at a ratio of 1 DC to 2 tumor cells for 3 h at 37°C in 5% CO_2 and washed three times with PBS before their use.

Human blood

Leukopaks were obtained from anonymous, healthy blood donors (New York Biologics). Per National Institutes of Health guidelines (https://grants.nih.gov/policy/humansubjects/research.htm), experiments with these cells were declared nonhuman subjects research by the UMMS Institutional Review Board.

Generation of MoDCs

DCs were generated from PBMCs prepared from leukopaks as previously described (McCauley et al., 2018). Briefly, to generate DCs, CD14^{+} mononuclear cells were isolated from PBMCs via positive selection using anti-CD14 Ab microbeads (Miltenyi). CD14^{+} cells were plated at a density of 2 × 10^6 cells/ml and cultured using RPMI-1640, supplemented with 5% heat-inactivated human AB^{+} serum (Omega Scientific), 1 mM sodium pyruvate, 20 mM GlutaMAX-I, 1× MEM nonessential amino acids, and 25 mM Hepes, pH 7.2 (RPMI–HS complete) in the presence of 1:100 cytokine-conditioned media containing human GM-CSF and human IL-4 for 6 d. DC preparations were consistently >99% DC-SIGN high, CD11c high, and CD14 low by flow cytometry.

Hydrophobically modified siRNA

Oligonucleotides targeting *Aim2* (mouse) or *AIM2* (human) were chemically modified in-house as described previously to generate *Aim2* and *AIM2* hydrophobically modified, fully chemically stabilized siRNAs (Hassler et al., 2018). *AIM2* siRNAs targeted the shared sequence of human and mouse AIM2 RNA. Table 2 lists chemical modification patterns and sequences of *Aim2* and *AIM2* siRNAs.

Transfection of BMDCs and MoDCs with siRNA

On day 5.5 during BMDC differentiation, floating cells were collected and plated at 10.5 × 10^6 cells (for in vivo experiments), 3.5 × 10^5 cells (for quantitative RT-PCR analysis and ELISA), or 1.4 × 10^6 cells (for Western blot analysis) in another 10-cm culture dish, 24-well plate, or 6-well plate, respectively. On day 6, BMDC medium was replaced with RPMI-1640 containing siRNA (35 nM) complexed with GeneSilencer Transfection Reagent (7 µl/ml; Genlantis) and incubated for 4 h. Subsequently, RPMI-1640, FBS, L-glutamine, 2-mercaptoethanol, GM-CSF, and IL-4 were added to the medium to create RPMI-1640 supplemented with 3% FBS, 2 mM L-glutamine, 50 µM 2-mercaptoethanol, 20 ng/ml GM-CSF, and 10 ng/ml IL-4. 48 h later, cells were harvested, washed twice with PBS, and used for quantitative RT-PCR analysis, Western blot analysis, ELISA, or generating

Table 2. **Chemical modifications and sequences of Aim2 hydrophobically modified siRNAs**

Name		Sequence
Aim2	Sense	(mU)#(mU)#(fU)(mG)(fU)(mA)(fA)(mA)(fA)(mG)(mU)(mU)(fU)#(mU)#(mA)-TegChol
siRNA 1	Antisense	P(mU)#(fA)#(mA)(fA)(fA)(fC)(mU)(fU)(mU)(fU)(mA)(fC)(mA)#(fA)#(mA)#(fG)#(mA)#(mA)#(mG)#(fA)
Aim2	Sense	(mG)#(mC)#(fU)(mG)(fA)(mA)(fA)(mG)(fC)(mU)(mA)(mU)(fA)#(mA)#(mA)-TegChol
siRNA 2	Antisense	P(mU)#(fU)#(mU)(fA)(fU)(fA)(mG)(fC)(mU)(fU)(mU)(fC)(mA)#(fG)#(mC)#(fA)#(mC)#(mC)#(mG)#(fU)
AIM2	Sense	(mG)#(mU)#(fU)(mG)(fA)(mA)(fU)(mU)(fA)(mU)(mA)(mU)(fG)#(mC)#(mA)-TegChol
siRNA 1	Antisense	P(mU)#(fG)#(mC)(fA)(fU)(fA)(mU)(fA)(mA)(fU)(mU)(fC)(mA)#(fA)#(mC)#(fU)#(mU)#(mC)#(mU)#(fG)
AIM2	Sense	(mU)#(mU)#(fU)(mG)(fU)(mA)(fA)(mA)(fA)(mG)(mU)(mU)(fU)#(mU)#(mA)-TegChol
siRNA 2	Antisense	P(mU)#(fA)#(mA)(fA)(fA)(fC)(mU)(fU)(mU)(fU)(mA)(fC)(mA)#(fA)#(mA)#(fG)#(mA)#(mA)#(mG)#(fA)
Control	Sense	(fU)#(mG)#(fA)(mC)(fA)(mA)(fA)(mU)(fA)(mC)(fG)(mA)(fU)#(mU)#(fA)-TegChol
siRNA	Antisense	V(mU)#(fA)#(mA)(fU)(mC)(fG)(mU)(fA)(mU)(fU)(mU)(fG)(mU)#(fC)#(mA)#(fA)#(mU)#(fC)#(mA)#(fU)

Note: Aim2 siRNA 1 and AIM2 siRNA 2 are single siRNAs that target mRNA sequence shared between mouse and human AIM2. Chemical modifications are designated as follows: m = 2′-O-methyl, f = 2′-fluoro, P = 5′-phosphate, and V = 5′-vinylphosphonate. #, phosphorothioate bond; (), phosphodiester bond; TegChol, 3′-tetraethylene glycol (Teg) cholesterol conjugate.

hgp100 peptide-pulsed DC vaccine. In some experiments, the medium of siRNA-transfected BMDCs was replaced with fresh BMDC medium every other day from 48-h later transfection and harvested 3, 10, or 22 d after transfection to perform RT-PCR analysis.

Similar to BMDC, on day 6 during MoDC differentiation, floating cells were collected and plated at 3.5×10^5 cells (for Western blot analysis and ELISA) in another 24-well plate and cultured in RPMI-1640 containing siRNA (35 nM) complexed with GeneSilencer Transfection Reagent (7 µl/ml) and incubated for 4 h Subsequently, RPMI-1640, FBS, L-glutamine, and 2-mercaptoethanol were added to the medium to create RPMI-1640 supplemented with 3% FBS, 2 mM L-glutamine, and 50 µM 2-mercaptoethanol. 48 h later, MoDCs were harvested, then left untreated for 6 h (nonprimed) or then primed for 6 h with LPS at a final concentration of 1 µg/ml, and used for Western blot analysis and ELISA.

Tumor models

B16F10 and YUMM1.7 melanoma cells (1.0×10^6) were resuspended in 100 µl PBS and implanted s.c. into the right flank of 6–12-wk-old WT and *Aim2*$^{-/-}$ mice. To examine tumor growth, tumor size was measured in two dimensions by calipers and is expressed as the product of two perpendicular diameters. Mice were euthanized on the days indicated in the figures. For all treatment experiments, mice were randomized for different treatments when the tumors were palpable. The combination of ACT and DC vaccination was performed in accordance with a modified version of a method described previously (Lou et al., 2004; Rashighi et al., 2014). PMELs were isolated from the spleens of PMEL mice through negative selection on microbeads (Miltenyi Biotec) in accordance with the manufacturer's instructions. After 7 d of tumor injection, purified PMELs (1.0×10^6 cells) and the whole bulk of cultured BMDCs pulsed with hgp100 peptide were injected i.v. into sublethally irradiated (500 rad, day −1) WT mice (day 0). The number of BMDCs was normalized to contain 1.0×10^6 hgp100 peptide-pulsed CD11c$^+$MHC-II$^+$ BMDCs to avoid the interexperimental variability of DC vaccination because of subtle differences in DC purity. Then, recombinant mouse IL-2 (R&D) was administered i.p. (6×10^4 U) once daily for 3 d consecutively from 1 d after vaccination. In experiments to analyze proliferation of PMELs in vivo, PMELs were labeled with 5 µM CFSE cell (Invitrogen) for 9 min at 37°C. In experiments to track vaccinated DCs, B6 CD45.1 hosts were used instead of WT (CD45.2) mice. In some experiments, 50 µl DNase I (Invitrogen; 1,000 U/ml) or 50 µl PBS was administered intratumorally every other day from 2 to 18 d after vaccination. For anti–PD-1 treatment experiments, WT mice were administered 250 mg of anti–PD-1 Ab (clone RMP1-14; BioXCell) or 250 mg of control isotype-matched Ab (clone 2A3; BioXCell) or 100 µl PBS i.p. on days 5, 8, 11, and 14. Furthermore, some WT mice were given 1.0×10^6 gp100 peptide-pulsed DC vaccine (DC-gp100) or 5.0×10^5 cDC1-TL i.v. on day 5 or the combination of DC vaccination and anti–PD-1 Ab on day 5 followed by anti–PD-1 Ab on days 8, 11, and 14 after B16F10 inoculation.

Flow cytometry

Tumor, tumor-draining inguinal LNs, and spleen were harvested at the indicated times. Draining LNs and spleen were disrupted by a 3-ml plunger, and cell suspensions were passed through 100-µm filters. The resected mouse tumor was minced with a razor blade and digested with collagenase D (1 mg/ml; Roche) and deoxyribonuclease I (0.5 mg/ml; Sigma-Aldrich) for 30 min in a 37°C shaking incubator (75 rpm). After enzymatic dissociation, the sample was transferred to ice to stop the reaction and was filtered through a 70-µm cell strainer. Red blood cells in the cell suspensions from tumor and spleen were lysed with ACK lysis buffer followed by washing with FACS buffer. The samples were then resuspended in FACS buffer. Cell suspensions were blocked with Fc block 2.4G2 (Bio X Cell) and stained with LIVE/DEAD Blue (1:1,000; Invitrogen) and relevant surface Abs at 4°C for 45 min. Subsequently, cells were washed twice and fixed with Cytofix/Cytoperm solution (BD Biosciences). For intracellular staining, relevant Abs diluted in Perm/Wash

Buffer (BD Biosciences) were applied to fixed cells and incubated for 30 min. Intracellular staining of FoxP3 was performed using FoxP3/Transcription Factor Staining kit (eBioscience) after surface staining. For intracellular cytokine staining, cells were stimulated with 12-myristate 13-acetate (PMA; 50 ng/ml; Sigma-Aldrich) and ionomycin (1 µg/ml; Sigma-Aldrich) in the presence of Brefeldin A (Biolegend) for 4 h before staining with Abs against cell surface molecules. After staining, cells were washed twice with FACS buffer. Data were collected with LSR II and analyzed with FlowJo software. In some experiments, CountBright Absolute Counting Beads (Thermo Fisher Scientific) were added to the samples in order to quantify the absolute DC number in each sample.

Abs specific to mouse CD45 (30-F11), CD45.1 (A20), CD45.2 (104), CD3 (17A2), CD4 (RM4-5), CD8a (53–6.7), Thy1.1 (OX-7), CD11c (N418), CD11b (M1/70), F4/80 (BM8), MHC-II (I-A/I-E; M5/114.15.2), MHC-I (H-2K^b/H-2D^b; 28–8-6), CD103 (2E7), CD80 (16-10A1), TNF-α (MP6-XT22), and IFN-γ (XMG1.2) were purchased from Biolegend. The Ab specific to mouse CD86 (GL-1) was purchased from Tonbo Biosciences, and the Ab specific to mouse FoxP3 (FJK-16s) was purchased from eBioscience. Abs specific to human CD11c (3.9), HLA-DR (L243), CD141 (M80), and CD1c (L161) were purchased from Biolegend. The above specific Abs were used for flow cytometry analysis, and fluorescence minus one controls were used to assist in gating.

Purification of tumor-derived DNA and stimulation of BMDCs and MoDCs

B16F10 DNA and human melanoma xenograft (melanoma DNA) was purified using the DNeasy Blood & Tissue Kit (Qiagen), following the manufacturer's instructions.

Human melanoma xenograft was established from the surgical specimen of primary tumor of one melanoma patient at the UMMS. Briefly, the patient-derived melanoma was minced and loaded into 1-cc syringes with 14-gauge needles. Subsequently, the tumor piece was inoculated s.c. at the right flank of NSG mice. After the mice developed a tumor of ∼10 × 10 × 10–mm size, the tumor was removed, and the portion of tumor was minced and used to extract melanoma DNA.

BMDCs were plated at 3.5 × 10^5 cells in 24-well plates (for quantitative RT-PCR analysis and ELISA) or 1.4 × 10^6 cells in 6-well plates (for Western blot analysis) and transfected with OPTI-MEM medium containing B16F10 DNA (0.1 or 1 µg/ml) complexed with Lipofectamine 2000 (1 µl/ml; Invitrogen). Similarly, MoDCs were plated at 3.5 × 10^5 cells in 24-well plates (for ELISA and Western blot analysis) and transfected with OPTI-MEM medium containing melanoma DNA (1 µg/ml) complexed with Lipofectamine 2000 (1 µl/ml).

ELISA

Tumor tissues, TdLNs, and spleens were homogenized in T-PER Tissue Protein Extraction Reagent (Thermo Fisher Scientific) supplemented with complete EDTA-free protease-inhibitor (Roche) and phosphatase inhibitor (PhosSTOP; Roche). Cell culture supernatants were obtained from BMDCs stimulated by B16F10 DNA for 4 h (IFN-β) and 10 h (CXCL10, IL-1β, and IL-18) and from siRNA-transfected LPS-primed MoDCs stimulated by human melanoma–derived DNA for 12 h (IFN-β, CXCL10, IL-1β, and IL-18). In some experiments, MoDCs were stimulated with human melanoma–derived DNA and 1 µM MCC950 (InVivoGen) for 12 h. The amount of IFN-β, IL-1β, and IL-18 in tumor, TdLN, and spleen lysates was measured with Mouse IFN Beta ELISA Kit, High Sensitivity (PBL Assay Science), Mouse IL-1β Duoset ELISA, and Mouse IL-18 Duoset ELISA (both R&D Systems), respectively. The concentrations of mouse IFN-β, CXCL10, IL-1β, and IL-18 in supernatants from BMDCs stimulated with B16F10 DNA were assessed using Mouse IFN-β Duoset ELISA, Mouse CXCL10 Duoset ELISA, Mouse IL-1β Duoset ELISA (all R&D Systems), and Mouse IL-18 ELISA Kit (Abcam), respectively. The concentration of human IFN-β, CXCL10, IL-1β, and IL-18 in supernatants from siRNA-transfected LPS-primed MoDCs stimulated with human-melanoma–derived DNA were assessed using human IFN-β Duoset ELISA, human CXCL10 Duoset ELISA, human CXCL10 Duoset ELISA, and human IL-18 Duoset ELISA Kit (all R&D Systems), respectively.

Peptide-pulsed DC vaccine–PMELs in vitro coculture assay

Peptide-pulsed DC vaccines (2.0 × 10^4 cells) that were stimulated with Lipofectamine (1 µl/ml) or B16F10 DNA (1 µg/ml) were cocultured with 1.0 × 10^5 CFSE-labeled PMELs at a 1:5 ratio in RPMI-1640 supplemented with 10% FBS (200 µl/well) in 96-well plates for 72 h. The amount of IFN-γ in the supernatant was measured by the Mouse IFN-γ Duoset ELISA (R&D), and the proliferation index of PMELs was measured by flow cytometry.

Quantitative RT-PCR analysis

Total RNA of mock-, control siRNA–, or *Aim2* siRNA–transfected WT BMDCs 2, 10, and 22 d after transfection and BMDCs stimulated with B16F10 DNA for 4 h were extracted with the use of an RNeasy Mini Kit (Qiagen). The RNA isolated from BMDCs was subjected to RT with the use of an iScript cDNA synthesis kit (Bio-Rad) followed by quantitative PCR analysis with the use of iQ SYBR Green Supermix (Bio-Rad) in an iCycler iQ (Bio-Rad), as previously described (Rashighi et al., 2014). Gene expression was normalized by the corresponding amount of β-actin mRNA. The sequences of the PCR primers (forward and reverse, respectively) were as follows: *Ifnb* (Ablasser et al., 2009) 5′–ATAAGCAGCTCCAGCTCCAA–3′, 5′–CTGTCTGCTGGTGGAGTTCA–3′; *Ifna* (Carroll et al., 2016) 5′–ATGGCTAGGCTCTGTGCTTTCCT–3′, 5′–AGGGCTCTCCAGACTTCTGCTCTG–3′; *Cxcl10* (Rashighi et al., 2014) 5′–AGGGGAGTGATGGAGAGAGG–3′, 5′–TGAAAGCGTTTAGCCAAAAAAGG–3′; *Cxcl9* (Rashighi et al., 2014) 5′–ATCTCCGTTCTTCAGTGTAGCAATG–3′, 5′–ACAAATCCCTCAAAGACCTCAAACAG–3′; *Aim2* (Brunette et al., 2012) 5′–GTTGAATCTAACCACGAAGTCC–3′, 5′–CTACAAGGTCCAGATTTCAACTG–3′; and *Actb* (Rashighi et al., 2014) 5′–GGCTGTATTCCCCTCCATCG–3′, 5′–CCAGTTGGTAACAATGCCATGT–3′.

Western blot analysis

Mouse BMDCs or human MoDCs were lysed in RIPA buffer (Thermo Fisher Scientific) supplemented with complete EDTA-free protease inhibitor and phosphatase inhibitor. The lysates were incubated for 30 min on ice and centrifuged at 15,000 ×*g* for 20 min at 4°C. The supernatants were denatured at 70°C for

10 min in NuPAGE LDS sample buffer (Life Technologies) with NuPAGE sample reducing agent (Life Technologies). Samples were separated by 3-(N-Morpholino) propanesulfonic acid–SDS Running Buffer (Life Technologies), and proteins were transferred onto a polyvinylidene difluoride membrane (Merck Millipore). Membranes were blocked in TBS with Tween 20 containing 4% nonfat dry milk for 2 h at room temperature followed by overnight incubation with anti-TBK1 (D1B4), anti-pTBK1 (D52C2), anti-IRF3 (D83B9), anti-pIRF3 (4D4G), anti-mouse AIM2, anti-human AIM2 (D5X7K), or anti-vinculin Ab (all from Cell Signaling Technology) primary Ab at 4°C. Immune complexes were detected with anti-rabbit IgG, HRP-linked secondary Ab (Cell Signaling Technology), ECL Prime Western Blotting Detection Reagents (GE Healthcare), and a LAS-4000 instrument (Fujifilm).

Immunohistofluorescence staining of human melanoma and quantification

Cases were selected randomly after approval by the Surveillance Committee for Human Subjects Research at the School of Medicine of Keio University. This study involved 31 patients treated at the Department of Dermatology of Keio University Hospital from 1995 to 2013. Diagnoses of malignant melanoma were confirmed histologically, and the study was designed to evaluate tumor thickness in primary lesions. The total follow-up period was 3–195 mo.

Tissue was fixed with 4% paraformaldehyde, embedded in paraffin, and sectioned at a thickness of 4 µm. Sections were paraffin depleted and rehydrated in a graded series of ethanol solutions. Sections were subjected to 10 min of microwave treatment in citrate buffer (pH 6.0) and were allowed to cool at room temperature. Nonspecific binding was blocked in 1% goat serum for 30 min at room temperature, and sections were incubated with the following primary Abs diluted in PBS with Tween 20: rabbit anti-AIM2 polyclonal Ab (eBioscience; 1:800) and mouse anti-CD11c mAb (2F1C10; Proteintech; 1:200), mouse anti-CD141 mAb (141C01; Invitrogen; 1:50), or mouse anti-CD1c mAb (OTI2F4; Abcam; 1:150) overnight at 4°C. After washing, binding of the AIM2 Abs was visualized with Alexa Fluor 568–labeled goat Abs to rabbit IgG (Invitrogen). Bindings of the CD11c, CD141, or CD1c Abs were visualized with Alexa Fluor 488–labeled goat Abs to mouse IgG (Invitrogen), and sections were mounted in VECTASHIELD HardSet Antifade Mounting Medium with DAPI (Vector laboratories). The uniformity of staining was confirmed each time by comparing stained samples with the s.c. fat tissue. Images were observed using the Zeiss Axio Observer (Carl Zeiss), collected with Axiovision software (ver. 4.8).

To evaluate stained samples, the focus of greatest inflammation was identified on each slide, and at least five contiguous 200× high-powered field (HPF) images were collected. Then, $CD11c^+$, $AIM2^+CD11c^+$, $CD141^+$, $AIM2^+CD141^+$, $CD1c^+$, and $AIM2^+CD1c^+$ cells infiltrating the tumor were quantified and averaged to estimate cell counts of these cells.

Study approval

All mice were housed in pathogen-free facilities at the UMMS, and procedures were approved under protocol #2266 by the UMMS Institutional Animal Care and Use Committee and in accordance with National Institutes of Health guidelines. Human melanoma samples were collected from patients examined by a dermatologist at UMMS and Keio University School of Medicine. The patients analyzed in this study were diagnosed with cutaneous melanoma and gave informed consent before study inclusion. Patient studies and human sample collection were performed according to protocols approved by the institutional review boards of UMMS and Keio University School of Medicine.

Statistics

Values are expressed as mean ± SEM. For tumor growth curve analysis, two-way ANOVA was performed with Tukey's or Sidak's multiple-comparisons test. Dual comparisons were made by Mann–Whitney test, and groups of three or more were compared by one-way ANOVA with Tukey's or Dunnett's multiple-comparisons test (for unpaired data) or the Friedman test with Dunn's multiple-comparisons test (for paired data). Statistically significant differences are indicated as follows: *, $P < 0.05$; **, $P < 0.01$; ***, $P < 0.001$; ****, $P < 0.0001$. GraphPad Prism7 software was used to perform analyses.

Online supplemental material

Fig. S1 shows the effects of host AIM2 deficiency on tumor, TdLN, and spleen in B16F10 and YUMM1.7 models. Fig. S2 shows the effect of AIM2-deficient DC vaccine with ACT on tumor, TdLN, and spleen in the B16F10 model. Fig. S3 shows the role of DNA sensing, IFNAR, and CXCL10 in AIM2-deficient DC vaccine with ACT on tumor, TdLN, and spleen in the B16F10 model. Fig. S4 shows the effect of IL-1β– and IL-18–deficient DC vaccine, as well as *Aim2* siRNA–transfected WT DC vaccine with ACT on tumor, TdLN, and spleen in the B16F10 model. Fig. S5 shows the effect of AIM2-deficient DC vaccine with anti–PD-1 immunotherapy on tumor, TdLN, and spleen in the B16F10 model.

Acknowledgments

We thank M. Bosenberg for providing YUMM1.7 cells and D. Golenbock for providing *Il1β*$^{-/-}$ mice. We also thank J. Richmond of the Harris Lab for technical assistance.

This study was supported by the National Institute of Arthritis and Musculoskeletal and Skin Diseases, part of the National Institutes of Health (grant AR069114 to J.E. Harris). Oligonucleotide synthesis was supported by National Institutes of Health instrumentation grant S10 OD020012 (to A. Khvorova).

Author contributions: K. Fukuda, K.A. Fitzgerald, and J.E. Harris designed the study. K. Fukuda, K. Okamura, R.L. Riding, X. Fan, K. Afshari, and N.-S. Haddadi performed the experiments. S.M. McCauley, M.H. Guney, and J. Luban provided human monocytes and human MoDCs. T. Funakoshi, T. Yaguchi, and Y. Kawakami provided human melanoma tissue samples. K.A. Fitzgerald provided *Aim2*$^{-/-}$ and *Sting*$^{-/-}$ mice. K.A. Fitzgerald and A. Khvorova designed and generated the control and *Aim2* hydrophobically modified siRNAs. K. Fukuda and J.E. Harris wrote the manuscript, and all authors read and edited the manuscript.

Disclosures: K. Fukuda, K.A. Fitzgerald, A. Khvorova, and J.E. Harris have filed a patent that covers AIM2 siRNAs and their use

to treat melanoma. The authors declare no other competing interests.

Submitted: 11 May 2020
Revised: 24 May 2021
Accepted: 9 July 2021

References

Ablasser, A., F. Bauernfeind, G. Hartmann, E. Latz, K.A. Fitzgerald, and V. Hornung. 2009. RIG-I-dependent sensing of poly(dA:dT) through the induction of an RNA polymerase III-transcribed RNA intermediate. *Nat. Immunol.* 10:1065–1072. https://doi.org/10.1038/ni.1779

Alcántara-Hernández, M., R. Leylek, L.E. Wagar, E.G. Engleman, T. Keler, M.P. Marinkovich, M.M. Davis, G.P. Nolan, and J. Idoyaga. 2017. High-Dimensional Phenotypic Mapping of Human Dendritic Cells Reveals Interindividual Variation and Tissue Specialization. *Immunity*. 47: 1037–1050.e6. https://doi.org/10.1016/j.immuni.2017.11.001

Anguille, S., E.L. Smits, E. Lion, V.F. van Tendeloo, and Z.N. Berneman. 2014. Clinical use of dendritic cells for cancer therapy. *Lancet Oncol.* 15: e257–e267. https://doi.org/10.1016/S1470-2045(13)70585-0

Anz, D., M. Rapp, S. Eiber, V.H. Koelzer, R. Thaler, S. Haubner, M. Knott, S. Nagel, M. Golic, G.M. Wiedemann, et al. 2015. Suppression of intratumoral CCL22 by type i interferon inhibits migration of regulatory T cells and blocks cancer progression. *Cancer Res.* 75:4483–4493. https://doi.org/10.1158/0008-5472.CAN-14-3499

Banerjee, I., B. Behl, M. Mendonca, G. Shrivastava, A.J. Russo, A. Menoret, A. Ghosh, A.T. Vella, S.K. Vanaja, S.N. Sarkar, et al. 2018. Gasdermin D Restrains Type I Interferon Response to Cytosolic DNA by Disrupting Ionic Homeostasis. *Immunity*. 49:413–426.e5. https://doi.org/10.1016/j.immuni.2018.07.006

Brinster, C., and E.M. Shevach. 2008. Costimulatory effects of IL-1 on the expansion/differentiation of CD4+CD25+Foxp3+ and CD4+CD25+Foxp3- T cells. *J. Leukoc. Biol.* 84:480–487. https://doi.org/10.1189/jlb.0208085

Brunette, R.L., J.M. Young, D.G. Whitley, I.E. Brodsky, H.S. Malik, and D.B. Stetson. 2012. Extensive evolutionary and functional diversity among mammalian AIM2-like receptors. *J. Exp. Med.* 209:1969–1983. https://doi.org/10.1084/jem.20121960

Carroll, E.C., L. Jin, A. Mori, N. Muñoz-Wolf, E. Oleszycka, H.B.T. Moran, S. Mansouri, C.P. McEntee, E. Lambe, E.M. Agger, et al. 2016. The Vaccine Adjuvant Chitosan Promotes Cellular Immunity via DNA Sensor cGAS-STING-Dependent Induction of Type I Interferons. *Immunity*. 44:597–608. https://doi.org/10.1016/j.immuni.2016.02.004

Corrales, L., S.R. Woo, J.B. Williams, S.M. McWhirter, T.W. Dubensky Jr., and T.F. Gajewski. 2016. Antagonism of the STING Pathway via Activation of the AIM2 Inflammasome by Intracellular DNA. *J. Immunol.* 196: 3191–3198. https://doi.org/10.4049/jimmunol.1502538

Corrales, L., V. Matson, B. Flood, S. Spranger, and T.F. Gajewski. 2017. Innate immune signaling and regulation in cancer immunotherapy. *Cell Res.* 27:96–108. https://doi.org/10.1038/cr.2016.149

Deng, L., H. Liang, M. Xu, X. Yang, B. Burnette, A. Arina, X.D. Li, H. Mauceri, M. Beckett, T. Darga, et al. 2014. STING-Dependent Cytosolic DNA Sensing Promotes Radiation-Induced Type I Interferon-Dependent Antitumor Immunity in Immunogenic Tumors. *Immunity*. 41:843–852. https://doi.org/10.1016/j.immuni.2014.10.019

DeYoung, K.L., M.E. Ray, Y.A. Su, S.L. Anzick, R.W. Johnstone, J.A. Trapani, P.S. Meltzer, and J.M. Trent. 1997. Cloning a novel member of the human interferon-inducible gene family associated with control of tumorigenicity in a model of human melanoma. *Oncogene.* 15:453–457. https://doi.org/10.1038/sj.onc.1201206

Fabbi, M., G. Carbotti, and S. Ferrini. 2015. Context-dependent role of IL-18 in cancer biology and counter-regulation by IL-18BP. *J. Leukoc. Biol.* 97: 665–675. https://doi.org/10.1189/jlb.5RU0714-360RR

Gaidt, M.M., T.S. Ebert, D. Chauhan, K. Ramshorn, F. Pinci, S. Zuber, F. O'Duill, J.L. Schmid-Burgk, F. Hoss, R. Buhmann, et al. 2017. The DNA Inflammasome in Human Myeloid Cells Is Initiated by a STING-Cell Death Program Upstream of NLRP3. *Cell.* 171:1110–1124.e18. https://doi.org/10.1016/j.cell.2017.09.039

Garg, A.D., P.G. Coulie, B.J. Van den Eynde, and P. Agostinis. 2017. Integrating Next-Generation Dendritic Cell Vaccines into the Current Cancer Immunotherapy Landscape. *Trends Immunol.* 38:577–593. https://doi.org/10.1016/j.it.2017.05.006

Gehrke, S., A. Otsuka, R. Huber, B. Meier, M. Kistowska, G. Fenini, P. Cheng, R. Dummer, K. Kerl, E. Contassot, and L.E. French. 2014. Metastatic melanoma cell lines do not secrete IL-1β but promote IL-1β production from macrophages. *J. Dermatol. Sci.* 74:167–169. https://doi.org/10.1016/j.jdermsci.2014.01.006

Goff, S.L., M.E. Dudley, D.E. Citrin, R.P. Somerville, J.R. Wunderlich, D.N. Danforth, D.A. Zlott, J.C. Yang, R.M. Sherry, U.S. Kammula, et al. 2016. Randomized, Prospective Evaluation Comparing Intensity of Lymphodepletion Before Adoptive Transfer of Tumor-Infiltrating Lymphocytes for Patients With Metastatic Melanoma. *J. Clin. Oncol.* 34:2389–2397. https://doi.org/10.1200/JCO.2016.66.7220

Hassler, M.R., A.A. Turanov, J.F. Alterman, R.A. Haraszti, A.H. Coles, M.F. Osborn, D. Echeverria, M. Nikan, W.E. Salomon, L. Roux, et al. 2018. Comparison of partially and fully chemically-modified siRNA in conjugate-mediated delivery in vivo. *Nucleic Acids Res.* 46:2185–2196. https://doi.org/10.1093/nar/gky037

Helft, J., J. Böttcher, P. Chakravarty, S. Zelenay, J. Huotari, B.U. Schraml, D. Goubau, and C. Reis e Sousa. 2015. GM-CSF Mouse Bone Marrow Cultures Comprise a Heterogeneous Population of CD11c(+)MHCII(+) Macrophages and Dendritic Cells. *Immunity*. 42:1197–1211. https://doi.org/10.1016/j.immuni.2015.05.018

Homet Moreno, B., J.M. Zaretsky, A. Garcia-Diaz, J. Tsoi, G. Parisi, L. Robert, K. Meeth, A. Ndoye, M. Bosenberg, A.T. Weeraratna, et al. 2016. Response to Programmed Cell Death-1 Blockade in a Murine Melanoma Syngeneic Model Requires Costimulation, CD4, and CD8 T Cells. *Cancer Immunol. Res.* 4:845–857. https://doi.org/10.1158/2326-6066.CIR-16-0060

Horai, R., M. Asano, K. Sudo, H. Kanuka, M. Suzuki, M. Nishihara, M. Takahashi, and Y. Iwakura. 1998. Production of mice deficient in genes for interleukin (IL)-1alpha, IL-1beta, IL-1alpha/beta, and IL-1 receptor antagonist shows that IL-1beta is crucial in turpentine-induced fever development and glucocorticoid secretion. *J. Exp. Med.* 187:1463–1475. https://doi.org/10.1084/jem.187.9.1463

Hou, Y., H. Liang, E. Rao, W. Zheng, X. Huang, L. Deng, Y. Zhang, X. Yu, M. Xu, H. Mauceri, et al. 2018. Non-canonical NF-κB Antagonizes STING Sensor-Mediated DNA Sensing in Radiotherapy. *Immunity*. 49:490–503.e4. https://doi.org/10.1016/j.immuni.2018.07.008

Ishikawa, H., and G.N. Barber. 2008. STING is an endoplasmic reticulum adaptor that facilitates innate immune signalling. *Nature.* 455:674–678. https://doi.org/10.1038/nature07317

Jones, J.W., N. Kayagaki, P. Broz, T. Henry, K. Newton, K. O'Rourke, S. Chan, J. Dong, Y. Qu, M. Roose-Girma, et al. 2010. Absent in melanoma 2 is required for innate immune recognition of Francisella tularensis. *Proc. Natl. Acad. Sci. USA*. 107:9771–9776. https://doi.org/10.1073/pnas.1003738107

Kakizaki, A., T. Fujimura, S. Furudate, Y. Kambayashi, T. Yamauchi, H. Yagita, and S. Aiba. 2015. Immunomodulatory effect of peritumorally administered interferon-beta on melanoma through tumor-associated macrophages. *OncoImmunology*. 4:e1047584. https://doi.org/10.1080/2162402X.2015.1047584

Kaplanski, G. 2018. Interleukin-18: Biological properties and role in disease pathogenesis. *Immunol. Rev.* 281:138–153. https://doi.org/10.1111/imr.12616

Kim, S.J., G. Kim, N. Kim, H. Chu, B.C. Park, J.S. Yang, S.H. Han, and C.H. Yun. 2019. Human CD141$^+$ dendritic cells generated from adult peripheral blood monocytes. *Cytotherapy*. 21:1049–1063. https://doi.org/10.1016/j.jcyt.2019.07.007

Krzastek, S.C., E. Goliadze, S. Zhou, A. Petrossian, F. Youniss, G. Sundaresan, L. Wang, J. Zweit, and G. Guruli. 2018. Dendritic cell trafficking in tumor-bearing mice. *Cancer Immunol. Immunother.* 67:1939–1947. https://doi.org/10.1007/s00262-018-2187-z

Lee, P.H., T.N. Yamamoto, D. Gurusamy, M. Sukumar, Z. Yu, J. Hu-Li, T. Kawabe, A. Gangaplara, R.J. Kishton, A.N. Henning, et al. 2019. Host conditioning with IL-1β improves the antitumor function of adoptively transferred T cells. *J. Exp. Med.* 216:2619–2634. https://doi.org/10.1084/jem.20181218

Li, K., S. Qu, X. Chen, Q. Wu, and M. Shi. 2017. Promising Targets for Cancer Immunotherapy: TLRs, RLRs, and STING-Mediated Innate Immune Pathways. *Int. J. Mol. Sci.* 18:404. https://doi.org/10.3390/ijms18020404

Lim, H.X., H.J. Hong, D. Cho, and T.S. Kim. 2014. IL-18 enhances immunosuppressive responses by promoting differentiation into monocytic myeloid-derived suppressor cells. *J. Immunol.* 193:5453–5460. https://doi.org/10.4049/jimmunol.1401282

Lou, Y., G. Wang, G. Lizée, G.J. Kim, S.E. Finkelstein, C. Feng, N.P. Restifo, and P. Hwu. 2004. Dendritic cells strongly boost the antitumor activity of

adoptively transferred T cells in vivo. *Cancer Res.* 64:6783–6790. https://doi.org/10.1158/0008-5472.CAN-04-1621

Lucarini, V., C. Buccione, G. Zicchedda, F. Peschiaroli, P. Sestili, R. Puglisi, G. Mattia, C. Zanetti, I. Parolini, L. Bracci, et al. 2017. Combining Type I Interferons and 5-Aza-2′-Deoxycitidine to Improve Anti-Tumor Response against Melanoma. *J. Invest. Dermatol.* 137:159–169. https://doi.org/10.1016/j.jid.2016.08.024

Ma, Z., W. Li, S. Yoshiya, Y. Xu, M. Hata, Y. El-Darawish, T. Markova, K. Yamanishi, H. Yamanishi, H. Tahara, et al. 2016. Augmentation of Immune Checkpoint Cancer Immunotherapy with IL18. *Clin. Cancer Res.* 22:2969–2980. https://doi.org/10.1158/1078-0432.CCR-15-1655

Man, S.M., R. Karki, and T.D. Kanneganti. 2016. AIM2 inflammasome in infection, cancer, and autoimmunity: Role in DNA sensing, inflammation, and innate immunity. *Eur. J. Immunol.* 46:269–280. https://doi.org/10.1002/eji.201545839

Mayer, C.T., P. Ghorbani, A. Nandan, M. Dudek, C. Arnold-Schrauf, C. Hesse, L. Berod, P. Stüve, F. Puttur, M. Merad, and T. Sparwasser. 2014. Selective and efficient generation of functional Batf3-dependent CD103+ dendritic cells from mouse bone marrow. *Blood.* 124:3081–3091. https://doi.org/10.1182/blood-2013-12-545772

McCauley, S.M., K. Kim, A. Nowosielska, A. Dauphin, L. Yurkovetskiy, W.E. Diehl, and J. Luban. 2018. Intron-containing RNA from the HIV-1 provirus activates type I interferon and inflammatory cytokines. *Nat. Commun.* 9:5305. https://doi.org/10.1038/s41467-018-07753-2

Mullins, D.W., S.L. Sheasley, R.M. Ream, T.N. Bullock, Y.X. Fu, and V.H. Engelhard. 2003. Route of immunization with peptide-pulsed dendritic cells controls the distribution of memory and effector T cells in lymphoid tissues and determines the pattern of regional tumor control. *J. Exp. Med.* 198:1023–1034. https://doi.org/10.1084/jem.20021348

Neller, M.A., J.A. López, and C.W. Schmidt. 2008. Antigens for cancer immunotherapy. *Semin. Immunol.* 20:286–295. https://doi.org/10.1016/j.smim.2008.09.006

Oertli, M., M. Sundquist, I. Hitzler, D.B. Engler, I.C. Arnold, S. Reuter, J. Maxeiner, M. Hansson, C. Taube, M. Quiding-Järbrink, and A. Müller. 2012. DC-derived IL-18 drives Treg differentiation, murine Helicobacter pylori-specific immune tolerance, and asthma protection. *J. Clin. Invest.* 122:1082–1096. https://doi.org/10.1172/JCI61029

Pace, L., S. Vitale, B. Dettori, C. Palombi, V. La Sorsa, F. Belardelli, E. Proietti, and G. Doria. 2010. APC activation by IFN-alpha decreases regulatory T cell and enhances Th cell functions. *J. Immunol.* 184:5969–5979. https://doi.org/10.4049/jimmunol.0900526

Pan, W., S. Zhu, K. Qu, K. Meeth, J. Cheng, K. He, H. Ma, Y. Liao, X. Wen, C. Roden, et al. 2017. The DNA Methylcytosine Dioxygenase Tet2 Sustains Immunosuppressive Function of Tumor-Infiltrating Myeloid Cells to Promote Melanoma Progression. *Immunity.* 47:284–297.e5. https://doi.org/10.1016/j.immuni.2017.07.020

Perez, C.R., and M. De Palma. 2019. Engineering dendritic cell vaccines to improve cancer immunotherapy. *Nat. Commun.* 10:5408. https://doi.org/10.1038/s41467-019-13368-y

Qin, Y., S. Ekmekcioglu, P. Liu, L.M. Duncan, G. Lizée, N. Poindexter, and E.A. Grimm. 2011. Constitutive aberrant endogenous interleukin-1 facilitates inflammation and growth in human melanoma. *Mol. Cancer Res.* 9:1537–1550. https://doi.org/10.1158/1541-7786.MCR-11-0279

Rashighi, M., P. Agarwal, J.M. Richmond, T.H. Harris, K. Dresser, M.W. Su, Y. Zhou, A. Deng, C.A. Hunter, A.D. Luster, and J.E. Harris. 2014. CXCL10 is critical for the progression and maintenance of depigmentation in a mouse model of vitiligo. *Sci. Transl. Med.* 6:223ra23. https://doi.org/10.1126/scitranslmed.3007811

Rathinam, V.A., Z. Jiang, S.N. Waggoner, S. Sharma, L.E. Cole, L. Waggoner, S.K. Vanaja, B.G. Monks, S. Ganesan, E. Latz, et al. 2010. The AIM2 inflammasome is essential for host defense against cytosolic bacteria and DNA viruses. *Nat. Immunol.* 11:395–402. https://doi.org/10.1038/ni.1864

Robert, C., A. Ribas, J. Schachter, A. Arance, J.J. Grob, L. Mortier, A. Daud, M.S. Carlino, C.M. McNeil, M. Lotem, et al. 2019. Pembrolizumab versus ipilimumab in advanced melanoma (KEYNOTE-006): post-hoc 5-year results from an open-label, multicentre, randomised, controlled, phase 3 study. *Lancet Oncol.* 20:1239–1251. https://doi.org/10.1016/S1470-2045(19)30388-2

Spranger, S., D. Dai, B. Horton, and T.F. Gajewski. 2017. Tumor-Residing Batf3 Dendritic Cells Are Required for Effector T Cell Trafficking and Adoptive T Cell Therapy. *Cancer Cell.* 31:711–723.e4. https://doi.org/10.1016/j.ccell.2017.04.003

Srivastava, S., M.A. Koch, M. Pepper, and D.J. Campbell. 2014. Type I interferons directly inhibit regulatory T cells to allow optimal antiviral T cell responses during acute LCMV infection. *J. Exp. Med.* 211:961–974. https://doi.org/10.1084/jem.20131556

Tian, T., S. Lofftus, Y. Pan, C.A. Stingley, S.L. King, J. Zhao, T.Y. Pan, R. Lock, J.W. Marglous, K. Liu, et al. 2020. IL1α Antagonizes IL1β and Promotes Adaptive Immune Rejection of Malignant Tumors. *Cancer Immunol. Res.* 8:660–671. https://doi.org/10.1158/2326-6066.CIR-19-0552

Tumeh, P.C., C.L. Harview, J.H. Yearley, I.P. Shintaku, E.J. Taylor, L. Robert, B. Chmielowski, M. Spasic, G. Henry, V. Ciobanu, et al. 2014. PD-1 blockade induces responses by inhibiting adaptive immune resistance. *Nature.* 515:568–571. https://doi.org/10.1038/nature13954

Villani, A.C., R. Satija, G. Reynolds, S. Sarkizova, K. Shekhar, J. Fletcher, M. Griesbeck, A. Butler, S. Zheng, S. Lazo, et al. 2017. Single-cell RNA-seq reveals new types of human blood dendritic cells, monocytes, and progenitors. *Science.* 356:eaah4573. https://doi.org/10.1126/science.aah4573

Wang, P.H., Z.W. Ye, J.J. Deng, K.L. Siu, W.W. Gao, V. Chaudhary, Y. Cheng, S.Y. Fung, K.S. Yuen, T.H. Ho, et al. 2018. Inhibition of AIM2 inflammasome activation by a novel transcript isoform of IFI16. *EMBO Rep.* 19:e45737. https://doi.org/10.15252/embr.201845737

Wculek, S.K., J. Amores-Iniesta, R. Conde-Garrosa, S.C. Khouili, I. Melero, and D. Sancho. 2019. Effective cancer immunotherapy by natural mouse conventional type-1 dendritic cells bearing dead tumor antigen. *J. Immunother. Cancer.* 7:100. https://doi.org/10.1186/s40425-019-0565-5

Wculek, S.K., F.J. Cueto, A.M. Mujal, I. Melero, M.F. Krummel, and D. Sancho. 2020. Dendritic cells in cancer immunology and immunotherapy. *Nat. Rev. Immunol.* 20:7–24. https://doi.org/10.1038/s41577-019-0210-z

Woo, S.R., M.B. Fuertes, L. Corrales, S. Spranger, M.J. Furdyna, M.Y. Leung, R. Duggan, Y. Wang, G.N. Barber, K.A. Fitzgerald, et al. 2014. STING-dependent cytosolic DNA sensing mediates innate immune recognition of immunogenic tumors. *Immunity.* 41:830–842. https://doi.org/10.1016/j.immuni.2014.10.017

Yang, J., S.P. Huck, R.S. McHugh, I.F. Hermans, and F. Ronchese. 2006. Perforin-dependent elimination of dendritic cells regulates the expansion of antigen-specific CD8+ T cells in vivo. *Proc. Natl. Acad. Sci. USA.* 103:147–152. https://doi.org/10.1073/pnas.0509054103

Zhou, Y., N. Slone, T.T. Chrisikos, O. Kyrysyuk, R.L. Babcock, Y.B. Medik, H.S. Li, E.S. Kleinerman, and S.S. Watowich. 2020. Vaccine efficacy against primary and metastatic cancer with in vitro-generated CD103$^+$ conventional dendritic cells. *J. Immunother. Cancer.* 8:e000474. https://doi.org/10.1136/jitc-2019-000474

Znidar, K., M. Bosnjak, M. Cemazar, and L.C. Heller. 2016. Cytosolic DNA Sensor Upregulation Accompanies DNA Electrotransfer in B16.F10 Melanoma Cells. *Mol. Ther. Nucleic Acids.* 5:e322. https://doi.org/10.1038/mtna.2016.34

JEM

Supplemental material

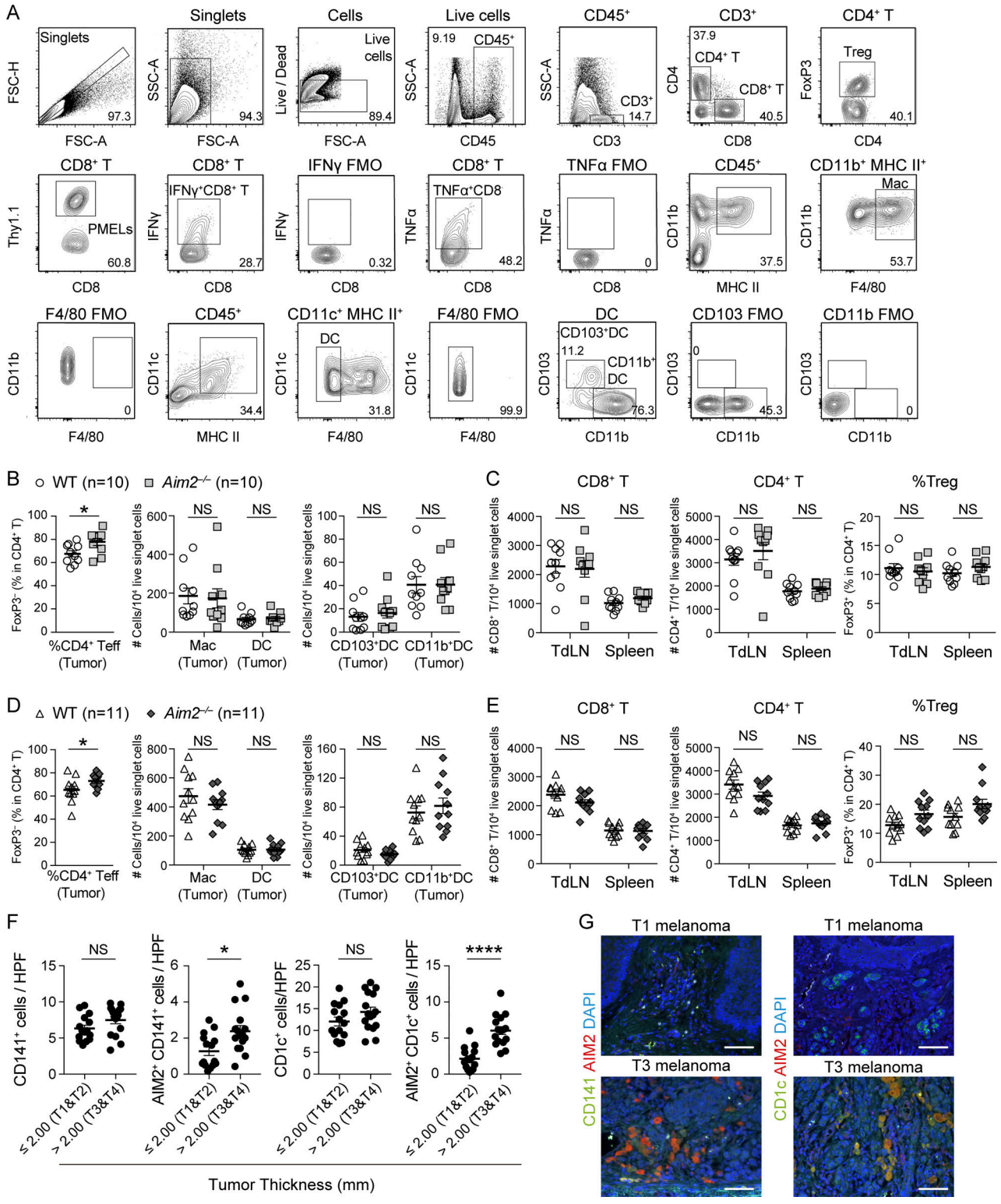

Figure S1. **Effects of host AIM2 deficiency on tumor, TdLN, and spleen in B16F10 and YUMM1.7 model. (A)** Gating strategy and representative flow cytometry plots for the assessment of indicated immune cells in B16F10 melanoma. FMO, fluorescence minus one control. **(B and C)** Flow cytometry analysis of the percentage of FoxP3$^-$ cells in total CD4$^+$ T cells, numbers of MACs, total DCs, CD103$^+$ DCs, and CD11b$^+$ DCs among 10^4 live singlet cells in the tumor (n = 10; B), numbers of CD8$^+$ and CD4$^+$ T cells among 10^4 live singlet cells, and percentages of FoxP3$^+$ cells in CD4$^+$ T cells in the TdLN and spleen (C) of WT and *Aim2*$^{-/-}$ mice 13 d after B16F10 s.c. inoculation. **(D and E)** Similar analysis as in B and C was performed on WT and *Aim2*$^{-/-}$ mice 17 d after YUMM1.7 melanoma inoculation (n = 11). **(F)** The numbers of CD141$^+$, AIM2$^+$CD141$^+$, CD1c$^+$, and AIM2$^+$CD141$^+$cells in HPF of primary lesions of human thin (n = 15) and thick (n = 16) melanomas. **(G)** Immunofluorescence microscopy of primary lesions of human thin and thick primary melanomas, visualized for CD141, CD1c, AIM2, and DAPI. Scale bar, 100 µm. Data are shown as mean ± SEM and are pooled from four (F) or three (B–E) independent experiments or are representative of four independent experiments (G). *, P < 0.05; ****, P < 0.0001; Mann–Whitney test (B–F).

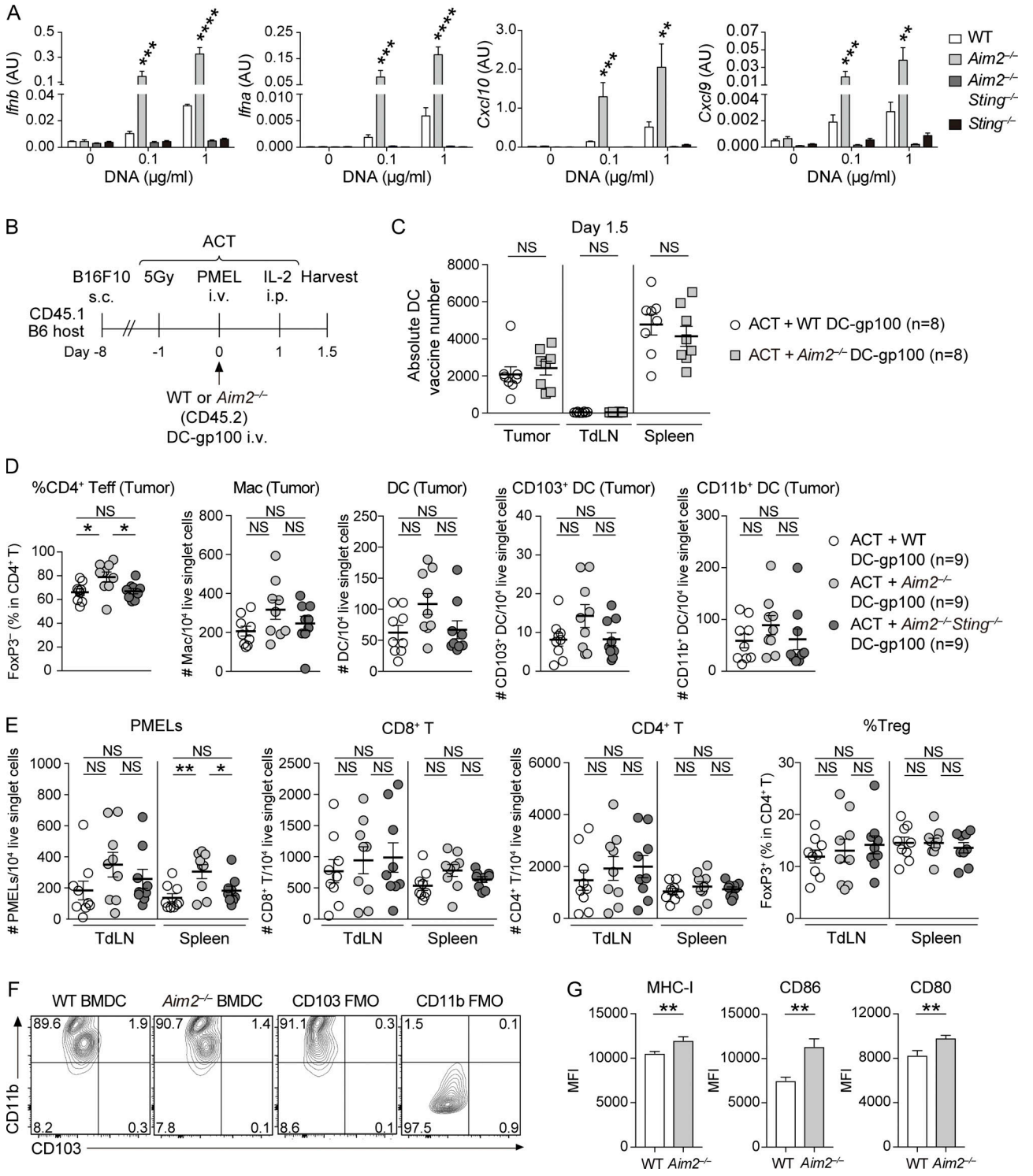

Figure S2. **The effect of AIM2-deficient DC vaccine with ACT on tumor, TdLN, and spleen in the B16F10 model. (A)** Quantitative RT-PCR analysis of *Ifnb*, *Ifna*, *Cxcl10*, and *Cxcl9* mRNA expression in indicated BMDCs stimulated with 0, 0.1, or 1 μg/ml B16F10 DNA for 4 h (n = 3), presented in AU, relative to *Actb* (encoding β-actin) expression. **(B)** Experimental scheme for analyzing DC vaccine infiltration in the tumor, TdLN, and spleen. B16F10-bearing CD45.1 congenic B6 mice were treated with ACT using 1.0 × 10^6 PMELs (CD45.2) + 1.0 × 10^6 WT or *Aim2*$^{-/-}$ DC-gp100 (CD45.2), and tissues were harvested 1.5 d after PMELs transfer. **(C)** The absolute numbers of transferred DCs present in the tumor, TdLN, and spleen (n = 8). **(D and E)** Flow cytometry analysis of the percentage of FoxP3$^-$ cells in total CD4$^+$ T cells, numbers of MACs, DCs, CD103$^+$ DCs, and CD11b$^+$ DCs among 10^4 live singlet cells in the tumor (D), numbers of PMELs, CD8$^+$ T cells, CD4$^+$ T cells among 10^4 live singlet cells, and percentages of FoxP3$^+$ cells in CD4$^+$ T cells in the TdLN and spleen (E) of B16F10 mice treated with ACT + WT, *Aim2*$^{-/-}$, or *Aim2*$^{-/-}$*Sting*$^{-/-}$ DC-gp100 (n = 9). **(F and G)** Flow cytometry staining of CD11b and CD103 (F) and the mean fluorescence intensity (MFI) of MHC class I (MHC-I), CD86, or CD80 (G) on freshly generated WT and *Aim2*$^{-/-}$ BMDCs (n = 8). Data are shown as mean ± SEM and are pooled from three (A and C–E) or two (G) independent experiments or are representative of two independent experiments (F). *, P < 0.05; **, P < 0.01; ***, P < 0.001; ****, P < 0.0001; one-way ANOVA with Dunnett's (A) or Tukey's (D and E) multiple-comparisons test or Mann–Whitney test (C and G). FMO, fluorescence minus one control.

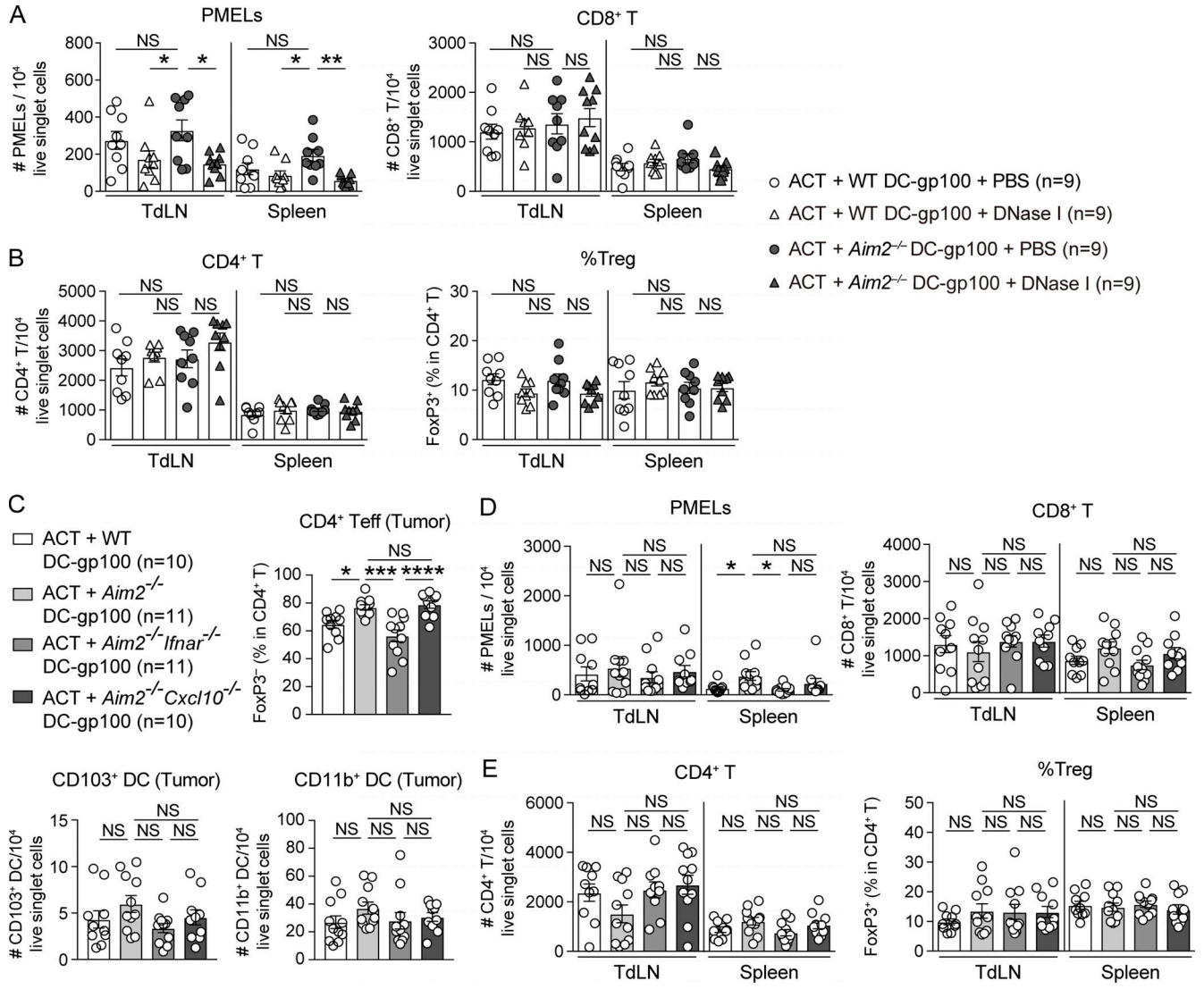

Figure S3. **The role of DNA sensing, IFNAR, and CXCL10 in AIM2-deficient DC vaccine with ACT on tumor, TdLN, and spleen in the B16F10 model. (A and B)** Flow cytometry analysis of the numbers of PMELs, CD8⁺ T cells (A), and CD4⁺ T cells among 10^4 live singlet cells and percentages of FoxP3⁺ cells in CD4⁺ T cells (B) in the TdLN and spleen of B16F10 mice treated with ACT + WT or *Aim2*$^{-/-}$ DC-gp100 and intratumoral administration of DNase I or PBS (n = 9). **(C–E)** Flow cytometry analysis of the percentage of FoxP3⁻ cells in total CD4⁺ T cells, numbers of CD103⁺ and CD11b⁺ DCs among 10^4 live singlet cells in the tumor (C), numbers of PMELs, CD8⁺ T cells (D), and CD4⁺ T cells among 10^4 live singlet cells and percentages of FoxP3⁺ cells in CD4⁺ T cells (E) in the TdLN and spleen of B16F10 mice treated with ACT + WT, *Aim2*$^{-/-}$, *Aim2*$^{-/-}$*Ifnar*$^{-/-}$, or *Aim2*$^{-/-}$*Cxcl10*$^{-/-}$ DC-gp100 (n = 10 or 11). Data are shown as mean ± SEM and are pooled from four (A and B) or three (C–E) independent experiments. *, P < 0.05; **, P < 0.01; ***, P < 0.001; ****, P < 0.0001; one-way ANOVA with Tukey's multiple-comparisons test (A–E).

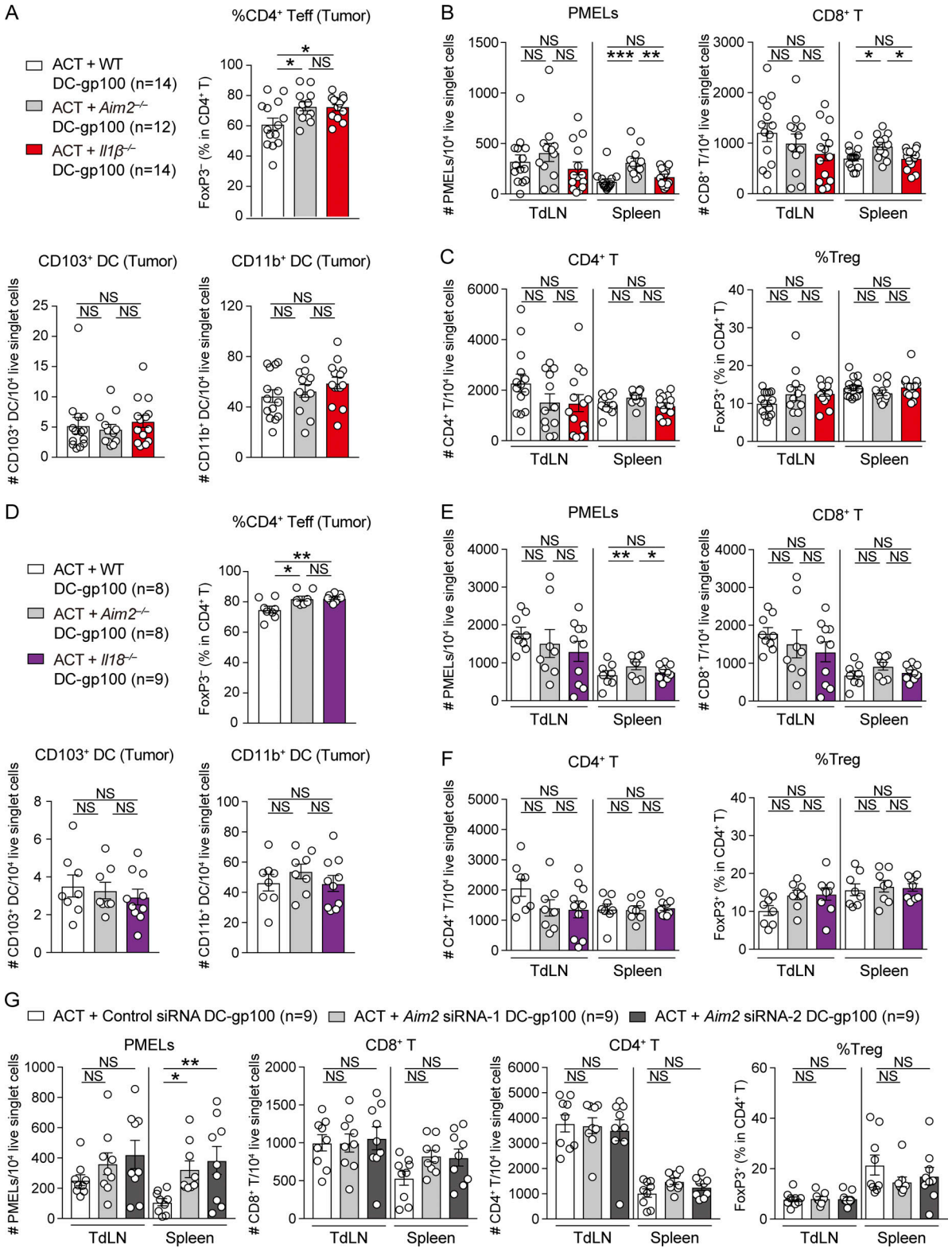

Figure S4. **Effect of IL-1β– and IL-18–deficient DC vaccine, as well as *Aim2* siRNA–transfected WT DC vaccine with ACT on tumor, TdLN, and spleen in the B16F10 model. (A–C)** Flow cytometry analysis of the percentage of FoxP3⁻ cells in total CD4⁺ T cells, numbers of CD103⁺ and CD11b⁺ DCs among 10^4 live singlet cells in the tumor (A), numbers of PMELs, CD8⁺ T cells (B), and CD4⁺ T cells among 10^4 live singlet cells, and percentages of FoxP3⁺ cells in CD4⁺ T cells (C) in the TdLN and spleen of B16F10 mice treated with ACT + WT, *Aim2*$^{-/-}$, or *Il1β*$^{-/-}$ DC-gp100 (n = 12–14). **(D–F)** Similar analysis as in A–C was performed on B16F10 mice treated with ACT + WT, *Aim2*$^{-/-}$, or *Il-18*$^{-/-}$ DC-gp100 (n = 9). **(G)** Flow cytometry analysis of the numbers of PMELs, CD8⁺ T cells, and CD4⁺ T cells among 10^4 live singlet cells and percentages of FoxP3⁺ cells in CD4⁺ T cells in the TdLN and spleen of B16F10 mice treated with ACT with control- or *Aim2* siRNA–transfected DC-gp100 (n = 9). Data are shown as mean ±SEM and are pooled from three (A–F) or two (G) independent experiments. *, P < 0.05; **, P < 0.01; ***, P < 0.001; one-way ANOVA with Tukey's (A–F) or Dunnett's (G) multiple-comparisons test.

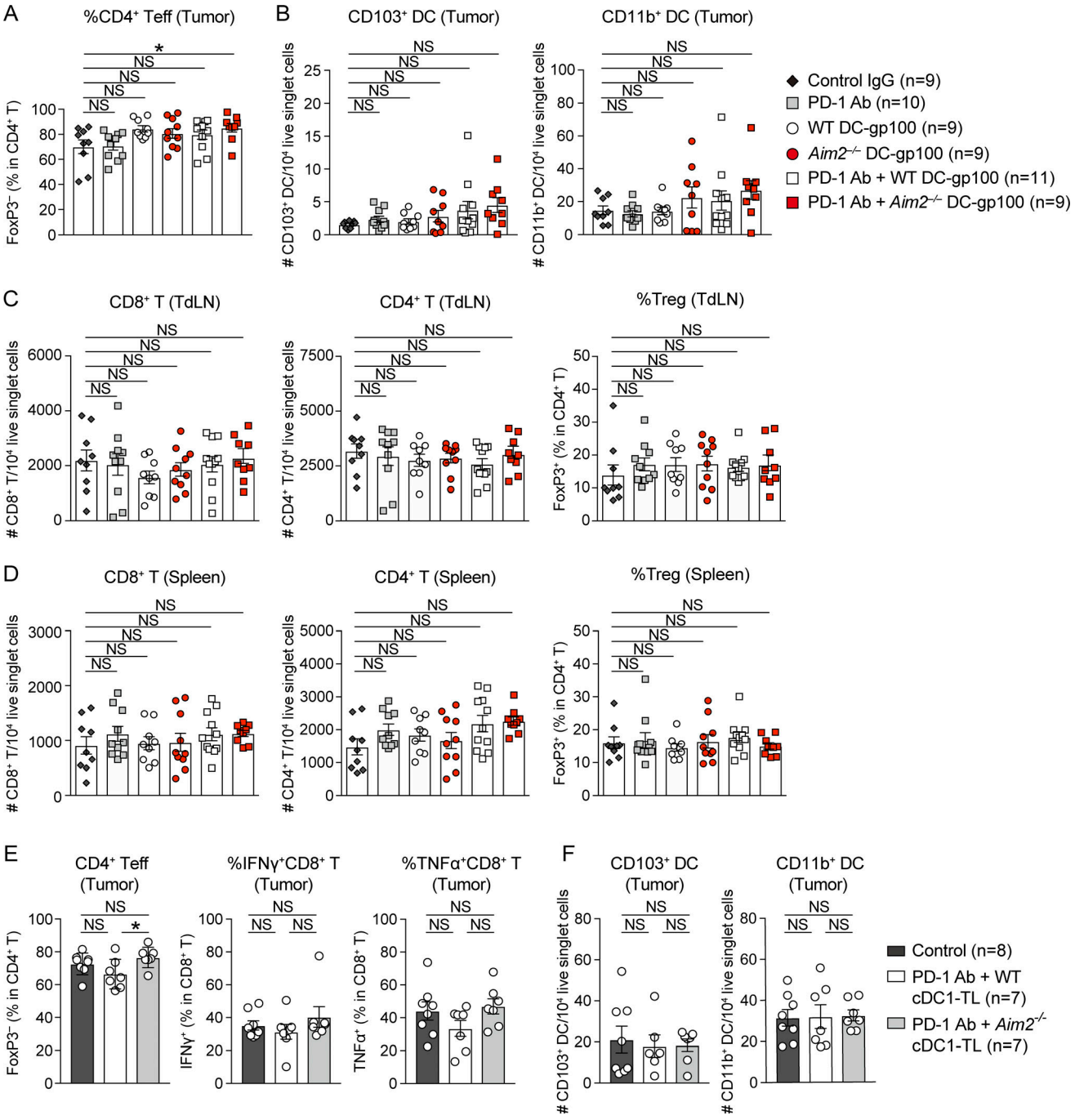

Figure S5. **Effect of AIM2-deficient DC vaccine with anti–PD-1 immunotherapy on tumor, TdLN, and spleen in the B16F10 model. (A–D)** Flow cytometry analysis of the percentage of FoxP3$^-$ cells in total CD4$^+$ T cells (A), numbers of CD103$^+$ and CD11b$^+$ DCs among 10^4 live singlet cells in the tumor (B), numbers of CD8$^+$ and CD4$^+$ T cells among 10^4 live singlet cells, and the percentages of FoxP3$^+$ cells in CD4$^+$ T cells in the TdLN (C) and spleen (D) of B16F10 mice treated by indicated therapies (n = 9–11). **(E and F)** Flow cytometry analysis of percentages of FoxP3$^-$ cells in total CD4$^+$ T cells, IFN-γ$^+$, and TNF-α$^+$ in CD8$^+$ T cells (E) and numbers of CD103$^+$ and CD11b$^+$ DCs among 10^4 live singlet cells (F) in the tumor of B16F10 mice treated by PBS (control), WT cDC1-TL + PD-1 Ab, or *Aim2*$^{-/-}$ cDC1-TL + PD-1 Ab (n = 7 or 8). Data are shown as mean ± SEM and are pooled from four (A–D) or two (E and F) independent experiments. *, P < 0.05; one-way ANOVA with Dunnett's (A–D) or Tukey's (E and F) multiple-comparisons test.